

---

# A Segmentation Algorithm for Measuring Blood Glucose in Hand-held Devices

---

Segmentierungsalgorithmus für die Messung von Glucose in Hand-Geräten

Bachelor-Thesis von Verónica Aramendía

6 March 2013

---



# A Segmentation Algorithm for Measuring Blood Glucose in Hand-held Devices Segmentierungsalgorithmus für die Messung von Glucose in Hand-Geräten

Vorgelegte Bachelor-Thesis von Verónica Aramendía

1. Gutachten: Nevine Demitri
2. Gutachten: Prof. Dr.-Ing. A. Zoubir

Tag der Einreichung:

---

# Declaration / Erklärung

To the best of my knowledge and belief this work was prepared without aid from any other sources except where indicated. Any reference to material previously published by any other person has been duly acknowledged. This work contains no material which has been submitted or accepted for the award of any other degree in any institution.

Hiermit versichere ich die vorliegende Arbeit ohne Hilfe Dritter nur mit den angegebenen Quellen und Hilfsmitteln angefertigt zu haben. Alle Stellen, die aus Quellen entnommen wurden, sind als solche kenntlich gemacht. Diese Arbeit hat in gleicher oder ähnlicher Form noch keiner Prüfungsbehörde vorgelegen.

Darmstadt, den 6. März 2013

---

(Verónica Aramendía)

---

# Abstract

This thesis deals with the estimation of blood glucose values from biomedical images. This estimation is related to the chemical reaction between glucose and a chemical reactant. The main goal is to segment the blood sample area from several sets of test measurements. An algorithm based on histograms thresholding and its combination with watershed segmentation is proposed and applied to these images. Furthermore, the kernel density estimator is used, as an alternative to the histogram, to estimate the probability density function of the images. After the identification of the optimal thresholding methods, a general procedure is proposed. This procedure includes image preprocessing, blood sample detection, histogram thresholding, binary masks comparison and a relative remission estimation. Then, using a convergence criterion the convergence value of the chemical reaction is found. Finally, the results are evaluated with respect to both accuracy and computation time.

---

# Abbreviations, Acronyms and Symbols

SE	Structuring Element
DM	Diabetes Mellitus
HBGM	Home Blood Glucose Monitoring
KDE	Kernel Density Estimation
MM	Mathematical Morphology
ROI	Region Of Interest
pdf	Probability density function
$A^c$	Complement of an image A
$\widehat{B}$	Reflection of an image B
$C_0, C_1$	Object and background classes
$C(n)$	Flooded catchment basin
$f$	Probability density function (pdf)
$\widehat{f}$	Estimate of the probability density function
h	Histogram
I	Image
$j_1, j_2$	Local maximums
K	Kernel function
L	Highest gray level
$M_i$	Regional minimum of the catchment basin
$n_l$	Number of pixels in an image with gray level l
$P_i$	A priori probability density function of a certain class i
q	Connected component from Q
Q	Set of connected components
rR	Relative remission
$\widehat{rR}$	Estimate of the relative remission
t	Time
$t_0$	Reaction time
$t_c$	Convergence time
T	Threshold
$T_{opt, OT}$	Optimal threshold for Otsu thresholding
$T_{opt, ME}$	Optimal threshold for minimum error thresholding
$T_{opt, INT}$	Optimal threshold for intermodes
$T_{opt, KDE}$	Optimal threshold for kernel density estimation thresholding method
w	Bandwidth of the kernel function
(x,y)	Spatial coordinates of an image
$\sigma_B^2$	Between-class variance
$\sigma_{TO}^2$	Total variance
$\sigma_{\widehat{rR}}^2$	Relative remission estimate variance
$\sigma_W^2$	Within-class variance

---

# Acknowledgments

First of all, I would like to thank my supervisor Nevine Demitri for giving me the chance of doing this bachelor thesis, and specially for her time and all her advices in this field of biomedical research. Especially, I want to thank my parents and boyfriend who unremittingly supported me during my year of studies in Germany. They made this work possible.

---

# Contents

<b>1</b>	<b>Introduction</b>	<b>1</b>
1.1	Diabetes And The Importance of Glucometers . . . . .	1
1.2	Glucometers Based on Photometric Principle . . . . .	1
1.3	Objective of the Thesis . . . . .	3
1.4	Structure of the Thesis . . . . .	4
<b>2</b>	<b>Methodology</b>	<b>6</b>
2.1	Morphological Image Processing . . . . .	6
2.1.1	Dilation and Erosion . . . . .	6
2.1.2	Opening and Closing . . . . .	7
2.1.3	Region Filling . . . . .	7
2.1.4	Connected Components . . . . .	8
2.2	Filters and Image Transformations . . . . .	9
2.2.1	Smoothing Linear Filters . . . . .	9
2.2.2	Order-statistics filters . . . . .	9
2.2.3	Power Law Transformations . . . . .	10
2.3	Histogram-based Thresholding. . . . .	10
2.3.1	Definition . . . . .	10
2.3.2	Otsu thresholding . . . . .	11
2.3.3	Minimum error thresholding . . . . .	12
2.3.4	Intermodes thresholding . . . . .	14
2.3.5	Limitations . . . . .	14
2.4	Kernel Density Estimation-based Thresholding . . . . .	14
2.5	Watershed Segmentation . . . . .	16
2.5.1	Watershed principle . . . . .	16
2.5.2	Dam Construction . . . . .	17
2.5.3	Watershed Segmentation Algorithm . . . . .	17
2.5.4	The Use of Markers . . . . .	17
2.5.5	The Distance Transform . . . . .	18
<b>3</b>	<b>Data Set</b>	<b>20</b>
3.1	Test Setup . . . . .	20
3.2	Artifacts . . . . .	21
<b>4</b>	<b>Proposed Algorithm and Evaluation</b>	<b>22</b>
4.1	Preprocessing . . . . .	22
4.2	Sample detection in device . . . . .	24
4.3	Masks calculation . . . . .	25
4.3.1	Evaluation of thresholding-based and segmentation methods . . . . .	26
4.4	Optimal Mask . . . . .	30



4.5 Relative remission calculation . . . . . 31

4.6 Convergence criterion . . . . . 32

**5 Experimental Results 34**

5.1 Otsu thresholding method . . . . . 34

5.2 Kernel density estimation-based thresholding method . . . . . 34

5.3 Watershed segmentation method . . . . . 37

**6 Conclusion and Outlook 44**

**7 Annex 45**



# List of Figures

1.1	An example of a glucometer, [4]. . . . .	2
1.2	Photometric principle. . . . .	3
1.3	Test strip structure. . . . .	4
1.4	Ideal kinetic model. . . . .	4
2.1	Region filling algorithm, [5]. . . . .	8
2.2	Connected components algorithm, [5]. . . . .	8
2.3	Smoothing kernels, [5]. . . . .	9
2.4	Power law curves, [5]. . . . .	10
2.5	KDE,[7]. . . . .	15
2.6	Watershed segmentation example. . . . .	16
2.7	Regional maximum and Regional minimum for a 550mg/dL example. . . . .	18
2.8	Distance transform, gradient and the imposed minimums for a 550mg/dL example. . . . .	18
2.9	Watershed segmentation and biggest connected component for a 550mg/dL example. . . . .	19
3.1	Different frames of a particular blood glucose frames. . . . .	20
3.2	Dust artifact. . . . .	21
3.3	Air bubble artifact. . . . .	21
4.1	General idea of the proposed algorithm. . . . .	22
4.2	Example of cropped and original frame. . . . .	22
4.3	Preprocessing Step. . . . .	24
4.4	SID Graph. . . . .	24
4.5	Sample in the device. . . . .	25
4.6	Histogram of exemplary images taken from different glucose values. . . . .	25
4.7	Masks calculation. . . . .	27
4.8	Problematic histogram for ME thresholding. . . . .	27
4.9	Histogram INT. Thresholding for a 550mg/dL frame. . . . .	28
4.10	Histogram INT. Thresholding for a 150 mg/dL SID frame. . . . .	28
4.11	Histogram KDE. Thresholding for a 150 mg/dL SID frame. . . . .	28
4.12	Mask from the different thresholding methods: 150 mg/dL. . . . .	29
4.13	Correct and incorrect thresholding of KDE for two different frames. . . . .	29
4.14	Watershed segmentation for high glucose values. . . . .	30
4.15	Watershed segmentation for low glucose levels. . . . .	30
4.16	Watershed segmentation for high glucose levels. . . . .	31
4.17	Optimal mask (550mg/dL), non-optimal mask(30mg/dL) and minimized SID mask. . . . .	31
4.18	Optimal mask. . . . .	32
4.19	Relative remission calculation. . . . .	32
4.20	Convergence criterion. . . . .	33
5.1	$\widehat{rR}$ for all glucose levels with Otsu. . . . .	37

5.2	OTSU Kinetik curve for all glucose levels. . . . .	38
5.3	$\widehat{rR}$ for all glucose levels with KDE. . . . .	40
5.4	KDE Kinetik curve for all glucose levels. . . . .	41
5.5	$\widehat{rR}$ for all glucose levels with Watershed segmentation. . . . .	42
5.6	Watershed segmentation Kinetik curve for all glucose levels. . . . .	43
7.1	Mask from the different thresholding methods: 30 mg/dL. . . . .	45
7.2	Mask from the different thresholding methods: 90 mg/dL. . . . .	45
7.3	Mask from the different thresholding methods: 150 mg/dL. . . . .	46
7.4	Mask from the different thresholding methods: 350 mg/dL. . . . .	46
7.5	Mask from the different thresholding methods: 550 mg/dL. . . . .	46
7.6	OTSU Kinetik curve 30 mg/dL. . . . .	47
7.7	OTSU Kinetik curve 90 mg/dL. . . . .	47
7.8	OTSU Kinetik curve 150 mg/dL. . . . .	48
7.9	OTSU Kinetik curve 350 mg/dL. . . . .	48
7.10	OTSU Kinetik curve 550 mg/dL. . . . .	49
7.11	KDE Kinetik curve 30 mg/dL. . . . .	49
7.12	KDE Kinetik curve 90 mg/dL. . . . .	50
7.13	KDE Kinetik curve 150 mg/dL. . . . .	50
7.14	KDE Kinetik curve 350 mg/dL. . . . .	51
7.15	KDE Kinetik curve 550 mg/dL. . . . .	51
7.16	Watershed segmentation Kinetik curve 150 mg/dL. . . . .	52
7.17	Watershed segmentation Kinetik curve 300 mg/dL. . . . .	52
7.18	Watershed segmentation Kinetik curve 550 mg/dL. . . . .	53

---

# List of Tables

1.1	Targets recommended for diabetics, [3]. . . . .	2
5.1	Otsu method: 30 mg/dL. . . . .	35
5.2	Otsu method: 90 mg/dL. . . . .	35
5.3	Otsu method: 150 mg/dL. . . . .	35
5.4	Otsu method: 350 mg/dL. . . . .	36
5.5	Otsu method: 550 mg/dL. . . . .	36
5.6	Otsu method: variance and computation time of the $\widehat{rR}$ . . . . .	36
5.7	TIME mask and SID mask of the $\widehat{rR}$ for high glucose levels. . . . .	36
5.8	Otsu method: mean of the convergence time for each glucose value. . . . .	36
5.9	KDE method: 30 mg/dL. . . . .	37
5.10	KDE method: 90 mg/dL. . . . .	38
5.11	KDE method: 150 mg/dL. . . . .	38
5.12	KDE method: 350 mg/dL. . . . .	39
5.13	KDE method: 550 mg/dL. . . . .	39
5.14	KDE method: variance and computation time of the $\widehat{rR}$ . . . . .	39
5.15	KDE method: Mean of the convergence time for each glucose value. . . . .	39
5.16	Watershed segmentation: 150 mg/dL. . . . .	40
5.17	Watershed segmentation: 350 mg/dL. . . . .	41
5.18	Watershed segmentation: 550 mg/dL. . . . .	41
5.19	Watershed segmentation: variance and computation time of the $\widehat{rR}$ . . . . .	42
5.20	Watershed segmentation: Mean of the convergence time for each glucose value. . . . .	42

---

# 1 Introduction

---

## 1.1 Diabetes And The Importance of Glucometers

---

According to [1], diabetes is expected to affect 552 million people of all age groups by 2030 worldwide and its prevalence is higher in men than women. Despite the fact that diabetes affects nearly 8.5% of the world's population, many people know very little about the disease.

According to the definition in [2], diabetes or diabetes mellitus denotes a condition, where the ability of controlling the body blood glucose is lost. Causes of diabetes can be linked to some facts such as being overweight or, inactive and it can also be more common in certain ethnic groups or have genetic reasons.

Glucose serves as a vital energy source for the human body, but organs can be damaged with high glucose levels over long periods of time. This is why the body of a non-diabetic person keeps control over its blood glucose levels. This way, glucose is absorbed when food is digested into the bloodstream and the levels rise. The pancreas, a gland beneath the stomach, responds by producing enough insulin to keep the blood glucose level under control. For diabetics, however, either the pancreas is unable to produce enough insulin or the body responds to the insulin poorly.

There are mainly two types of diabetes:

- **Type 1 diabetes:** One out of 10 diabetics has type 1 diabetes. This type of diabetes usually begins earlier in life. The pancreas stops producing insulin and it is more common in younger people. Treatments involve changes in the patients diet, and taking insulin either with an injection pen or using an insulin pump.
- **Type 2 diabetes:** 9 out of 10 diabetics have type 2 diabetes. This type of diabetes usually starts later in life, and sometimes it can be controlled with exercise and changes in the diet. Here although the pancreas is producing insulin, it is not enough to meet the body needs or it is not used properly.

For both types of diabetes frequent measuring of the blood glucose levels is vitally important. According to [2], a glucometer is a medical device that determines the approximate concentration of glucose in the blood by reading a small blood sample placed on a disposable test strip obtained pricking the skin with a lancet. The test strip contains a chemical agent that reacts with the glucose in the blood sample. Figure 1.1 shows an example of a glucometer.

Diabetics, typically, check their blood sugar before and after the meals. The targets recommended for blood glucose levels for most diabetics are shown in Table 1.1.

---

## 1.2 Glucometers Based on Photometric Principle

---

The photometric principle is a common method to measure the glucose concentration from a blood sample. It is based on the detection of reflected light which changes according to the color reaction of

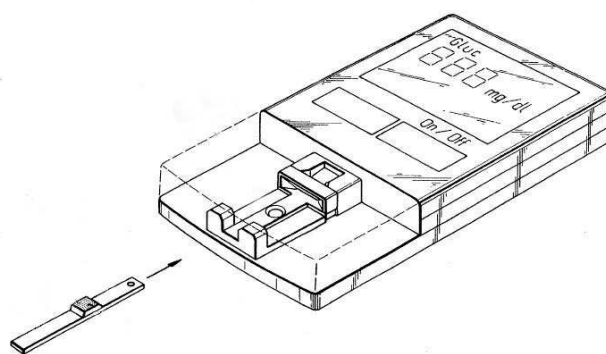


**Figure 1.1:** An example of a glucometer, [4].

Time of the day	Target blood glucose levels
Before meals	70 to 130 mg/dL
1 to 2 hours after the start of a meal	Less than 180 mg/dL

**Table 1.1:** Targets recommended for diabetics, [3].

a chemical agent due to its reaction with the blood glucose. Normally, several LEDs are used to achieve a homogeneous lighting on the evaluation area where we can find the chemical substance that reacts with the glucose. A blood sample is taken from the patient and placed on it. The chemical reaction takes place yielding a color formation. Hence, the more glucose in the blood, the larger the color change taking place. This color reflection is captured by a sensor that subsequently can be mapped to the glucose value of the region of interest. We can assume that all the reflected light coming from the chemical field belongs to the reflections by the chemical reaction if the blood sample is big enough to cover all the evaluation area. Figure 1.2 shows an image explaining the photometric principle.

To reduce the pain for the patient, a smaller blood sample can be used. This leads to the problem that the color reflection obtained from the LEDs is not only associated to the blood sample but also to the dry areas around it. By capturing the reflected light using just one sensor, the reflections will originate not only from the test field but also from the background so it cannot be assumed that it is directly related to the color change. Therefore, this is then by a camera during approximately 5-10s. The results are given as sets of images that describe the temporal behavior of the chemical reaction over the whole test strip.

To test this principle, a measurement setup that works with different glucose values has been used. The initial samples have been achieved using a glucose solution. These test measurements are observed during 20s and make us able to test the device under different circumstances. The images are degraded by many factors, such as noise or air bubbles what can lead to distorted results of blood glucose. The main objective is to find the area where the blood sample is and perform appropriate filtering to be able to assess the glucose value accurately.

In Figure 1.3 we can see the test strip structure where the blood sample is placed. Its shape is based on basically two channels separated by a bridge, that enables a uniform blood spread over the channels. All test strip dimensions are known.

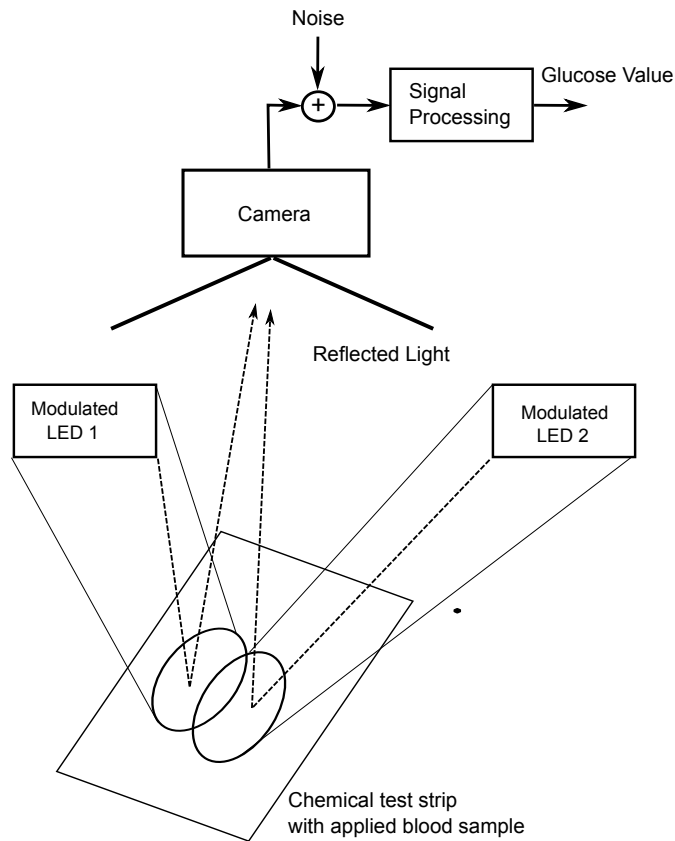


**Figure 1.2:** Photometric principle.

In order to take into account the time behavior of the chemical reaction, the ideal kinetics model should be observed. In Figure 1.4 the reflected light over the reaction time  $t$  is presented for both high and low glucose levels. The relative remission is defined as the quotient of the amount of reflected light from the LED to the initial amount of reflected light before the reaction.

In Figure 1.4, it can be observed that for the time  $t < t_0$  the relative remission keeps a constant intensity level at the maximum value due to the fact that the blood sample requires a certain time to be detected by the device. At  $t_0$  a large drop in the chemical reaction can be observed, the blood sample has been detected. The reaction behavior acts like an inverse exponential function and reaches a convergence point at a particular time,  $t_c$ . It can be seen that high glucose levels have a stronger color reaction and thus are related to a lower relative remission, in contrast to samples with lower glucose levels. The point where the reaction converges yields the corresponding estimated glucose value of the used concentration. This point is the third one whose difference between two consecutive frames is less than 1%. Here, the points below  $t_0$  are not taking into account due to the fact that the color reaction is still happening.

---

### 1.3 Objective of the Thesis

---

This thesis introduces analysis methods, which focus on detecting the convergence frame and on segmenting and filtering the relevant part of the digital image where the reaction takes place. This is the region of interest, ROI. Once this is found, the mean of this relevant area is taken and can be mapped via

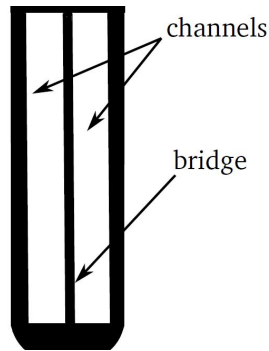


**Figure 1.3:** Test strip structure.

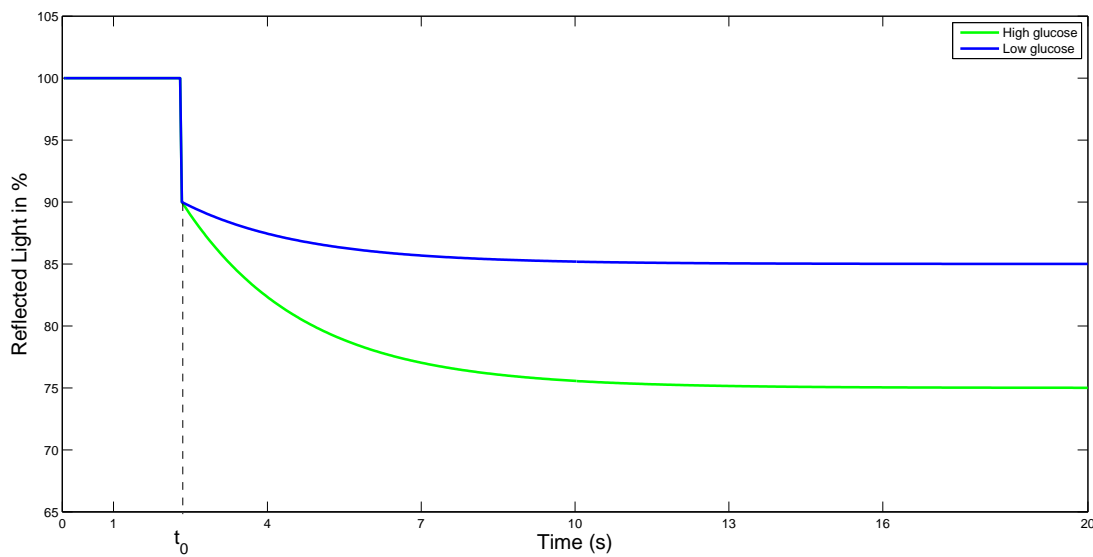


**Figure 1.4:** Ideal kinetic model.

a mapping function to obtain the corresponding glucose values. Different methods and their execution times are compared and evaluated.

## 1.4 Structure of the Thesis

**Chapter 2** introduces the used methodology from basic morphological preprocessing methods to different segmentation procedures.

**Chapter 3** presents the image data sets and the test setup employed. Furthermore, we present some of the possible artifacts that may affect our sample images.

**Chapter 4** forms the main part of the thesis by describing the proposed algorithm with the different segmentation methods and their evaluation.

**Chapter 5** presents the experimental results of the optimal methods, followed by a comparison of those with their advantages and disadvantages.

**Chapter 6** forms a conclusion of the report and provides a short outlook for further work.

**Chapter 7** is an annex that includes some of the images used in the thesis.

---

This project has been performed in cooperation with the company Roche Diagnostics GmbH at Mannheim, Germany. The method has been modeled within Matlab.



---

## 2 Methodology

This chapter first gives a brief overview of the basic morphological operators for both image processing and image segmentation. Furthermore, an insight on image filters, image transformations and different segmentation procedures is given.

---

### 2.1 Morphological Image Processing

---

According to [5], *morphology* is a term that denotes several branches that deal with the structure and forms of some identities. *Mathematical Morphology* (MM) in particular, is a theory used for the analysis and processing of geometrical structures in order to extract image components that are useful in the representation and description of region shape, such as boundaries, skeletons, and the convex hull.

*Set theory* is the language of mathematical morphology, where *sets* represent the objects in an image. For example, a gray scale digital image is a set with two components of each element referring to the coordinates of a pixel, and the third referring to its discrete gray-level value. However, sets can contain other image or video attributes, such as color and time variations. So mathematical morphology is based on a fundamental binary relation between an object and a set.

---

#### 2.1.1 Dilation and Erosion

---

The basic operator needed to work with mathematical morphology is usually referred as a *Structuring Element*(SE) and it is denoted by  $B$ . The SE is a shape with a certain size chosen due to a priori-knowledge of the image and used to probe or interact with the image  $A$  in order to obtain some conclusions on how it fits.

---

##### Dilation

---

*Dilation* can be compared to a convolution process, where the set  $B$  is viewed as a convolution mask that is flipped around its origin and slid over the image  $A$ . The dilated set is, then, the set of points that is covered by  $B$ , as the center of  $B$  slides through the image  $A$ . The final effect of dilation is the expansion of the set  $A$  [5]. Considering  $A$  and  $B$  sets in  $\mathbb{Z}^2$ , the *dilation* of  $A$  by  $B$  can be denoted  $A \oplus B$  and is defined as:

$$A \oplus B = \{z \mid (\hat{B})_z \cap A \neq \emptyset\} \quad (2.1)$$

---

##### Erosion

---

*Erosion*, leads to the contrary effect. The eroded set is the set of points formed, when the *SE* is fully inside the set  $A$ , as the center of  $B$  slides through  $A$ . Therefore, it leads to a shrinking of the set  $A$ . For sets  $A$  and  $B$  in  $\mathbb{Z}^2$ , the erosion of  $A$  by  $B$  is denoted  $A \ominus B$  and is therefore defined as:

$$A \ominus B = \{z \mid (B)_z \subseteq A\} \quad (2.2)$$

In other words, this equation indicates that the erosion of A by B is the set of all points of z such that B, translated by z, is contained in A.

---

### 2.1.2 Opening and Closing

---

In this subsection concepts about *opening and closing* derived from the previous ones are explained. The first, generally smooths the contour of an object, by eliminating thin protrusions. It is somewhat like erosion in that it tends to remove some of the foreground (bright) pixels from the edges of regions. However, in general it is less destructive than erosion. Closing is similar in some ways to dilation in that it tends to enlarge the boundaries of foreground (bright) regions in an image, eliminating small holes, and filling gaps in the contour. It is also less destructive.

The *opening* of set A by the structuring element B, denoted  $A \circ B$ , is defined as:

$$A \circ B = (A \ominus B) \oplus B \quad (2.3)$$

Similarly, the *closing* of set A by structuring element B, denoted  $A \bullet B$ , is defined as:

$$A \bullet B = (A \oplus B) \ominus B \quad (2.4)$$

Opening and closing are duals of each other with respect to set complementation and reflection, what can be showed in the next equation.

$$(A \bullet B)^c = (A^c \circ \widehat{B}) \quad (2.5)$$

---

### 2.1.3 Region Filling

---

*Region filling* is a simple algorithm based on a set of dilations, complementation, and intersections. It uses a random set containing a subset whose elements are 8-connected boundary points of a region. The start point is called seed and it must be one inside the boundary. The objective is to fill the entire region with 1's in the following interactions. To start with, it is assumed that all non boundary points are labeled 0. Considering an image A and a structuring element B represented in Figure 2.1, the procedure is the following:

$$X_k = (X_{k-1} \oplus B) \cap A^c, \quad k = (1, 2, 3 \dots n) \quad (2.6)$$

where k is the number of iterations,  $X_k$  is the resulting image after the kth iteration, and the first resulting iteration fits in with the starting point  $X_0 = \text{seed}$ .

If  $X_k = X_{k-1}$  the algorithm finishes. The set union of  $X_k$ , and A contains the filled set and its boundary. The intersection at each step with  $A^c$  is what limits the result to inside the region of interest.

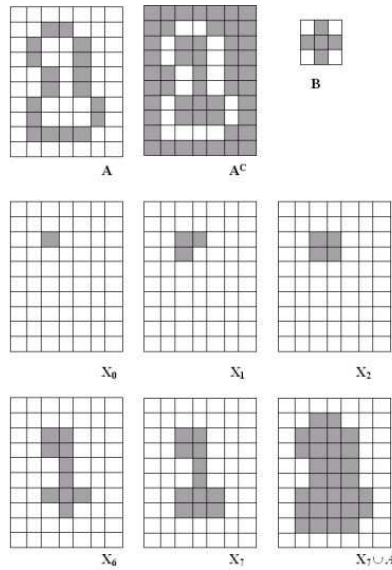


Figure 2.1: Region filling algorithm, [5].

### 2.1.4 Connected Components

Given a starting point, seed, inside an object we can use the same principle as in region filling with a slight modification. Let's consider the image  $A$ , an optimal structuring element  $B$  represented in Figure 2.2 and an element  $q$  of a set  $Q$  of connected components contained in  $A$ . The difference with respect region filling is that since the object now is defined by ones (and not zeros surrounded by a contour),  $A$  does not have to be inverted. According to [5] connected components algorithm follows the next iterative process:

$$X_k = (X_{k-1} \oplus B) \cap A, \quad k = (1, 2, 3...n) \quad (2.7)$$

where  $X_0 = \text{seed}$  and taking into account that the algorithm converges when  $X_k = X_{k-1}$  and  $q = X_k$ .

After scanning all the image, in order to identify connected pixel regions, we analyze the size of the objects that remain. We label these objects by extracting the connected components in the image, and different measures of connectivity are possible. Then, we determine significant foreign objects that are contained in the original image.

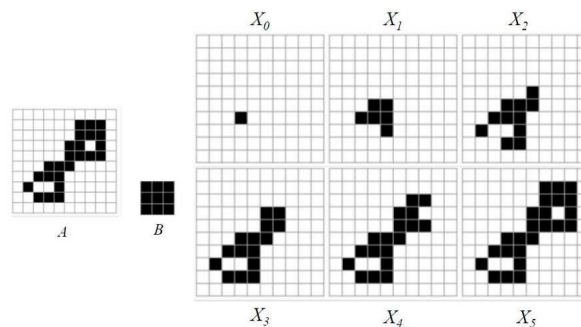


Figure 2.2: Connected components algorithm, [5].

---

## 2.2 Filters and Image Transformations

---

This subsection starts by introducing smoothing linear filters and order-statistics filters. We use them to eliminate small objects such as noise, in order to clear the image and segment it reliably.

---

### 2.2.1 Smoothing Linear Filters

---

Spatial smoothing means that data points contained in the neighborhood of the filter mask are averaged. This has the effect of a low pass filter meaning that high frequencies of the signal are removed from the data while enhancing low frequencies. The result is that sharp 'edges' of the images are blurred and spatial correlation within the data is more pronounced. Blurring is, often, desired for ease of object detection.

Another obvious application of smoothing is noise reduction, because random noise typically consists of sharp transitions in gray levels. However, edges correspond to high frequencies too, and they are desirable features of an image [5]. The smoothing kernels must all have positive weights and they can be any size. In Figure 2.3 we can see that the most typical ones are 3x3 kernels.

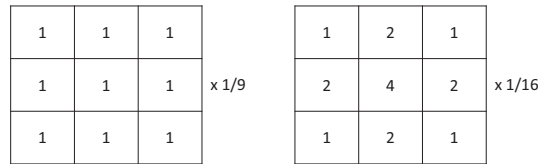


Figure 2.3: Smoothing kernels, [5].

---

### 2.2.2 Order-statistics filters

---

*Order-statistics filters* are nonlinear spatial filters. Their final response is based on ranking the pixels contained in the image area encompassed by the filter. After that, the center pixel value is replaced with the one determined by the ranking result.

One of the filters used in this thesis is the median filter, which, as its name implies, replaces the value of a pixel by the median of the gray levels in the neighborhood of that pixel. The original value of the pixel is also included in the computation of the median. Median filters are particularly effective in the presence of impulse noise, also called '*salt-and-pepper*' noise because of its appearance as white and black dots superimposed on an image [5]. They provide considerably less blurring than linear smoothing filters of similar size. Considering  $S_{x,y}$  the set of coordinates in a rectangular subimage centered at point  $(x, y)$ , the median filter computes the median value of the corrupted image  $I(x, y)$  in the area defined by  $S_{x,y}$ . The value of the restored image  $I_{rest}(x, y)$  is:

$$I_{rest}(x, y) = \text{median}_{(s,t) \in S_{(x,y)}} \{I(s, t)\} \quad (2.8)$$

The main disadvantage of order statistics filters and, particularly, their repeated iterations, is the high computational complexity associated with their implementation.

---

### 2.2.3 Power Law Transformations

---

Power law transformations have the basic form:  $s = c \cdot r^\gamma$  where  $c$  and  $\gamma$  are positive constants and  $r$  and  $s$  are the input and output gray levels respectively. Sometimes the formula is written to account for an offset, but they are usually an issue of display calibration and consequently, normally ignored. Plots of  $s$  versus  $r$  for various values of  $\gamma$  are shown in Figure 2.4.

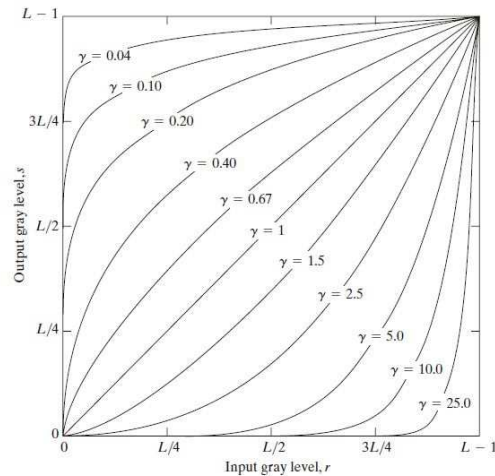


Figure 2.4: Power law curves, [5].

Power-law curves with fractional values of  $r$  map a narrow range of dark input values into a wider range of output values, with the opposite being true for higher values of input levels. One of its possible image processing applications is highlighting and giving contrast to images.

---

## 2.3 Histogram-based Thresholding.

---

According to [5], segmentation can be defined by the process of partitioning a digital image into multiple segments by labeling every pixel according to a certain characteristic. Its aim is to modify the representation of an image into something more meaningful to analyze. Typically it is used for the location of objects and boundaries such as lines and curves in images.

Several techniques have been developed for this purpose but since there is no general solution to the image segmentation problem, these methods often have to be combined with other domain knowledge in order to effectively solve an image segmentation problem.

One possible technique is thresholding the histogram of an image to segment it. In this section we give a brief definition about histograms based on thresholding, and after that some detail about different thresholding algorithms such as Otsu, minimum error or intermodes.

---

### 2.3.1 Definition

---

Histograms are the basis for numerous spatial domain processing techniques. Not only do they have a simple software calculation but they also permit economic hardware implementations, therefore they have become an important tool in real time image processing. Furthermore, histograms can be effectively

manipulated for different processing applications, such as image enhancement, image compression and segmentation.

In [5] the histogram  $h$  of a digital image with gray levels in the range  $(0, L - 1)$  where  $L$  is the highest one, is defined as a discrete function  $h(l) = n_l$ , where  $l$  is the  $l$ th gray level and  $n_l$  is the number of pixels in the image having gray level  $l$ . Then, the total number of pixels,  $n$ , in a given image is:

$$n = \sum_{l=0}^{L-1} n_l \quad (2.9)$$

It is common to normalize a histogram in order to make it independent from the dimensions of the image. To normalize it, each of its values is divided by the total number of pixels in the image, denoted by  $n$ . Finally, a normalized histogram is given by  $h_{\text{norm}}(l) = n_l/n$  for  $l = (0, \dots, L - 1)$ . Loosely speaking,  $h_{\text{norm}}(l)$  gives an estimate of the probability of occurrence of gray level  $l$  where the sum of all components of a normalized histogram is equal to 1.

Defining  $(x, y)$  as the spatial coordinates of a digitized image, and  $G = (0, 1, \dots, L - 1)$  as a set of positive integers representing gray levels, the image function can be defined as  $I(x, y) \in G$ . Let  $T \in G$  be a threshold so that the thresholded image  $I_{\text{thres}}(x, y)$  is defined as:

$$I_{\text{thres}}(x, y) = \begin{cases} 0 & \text{if } I(x, y) < T \\ 1 & \text{if } I(x, y) \geq T \end{cases} \quad (2.10)$$

Thus, pixels labeled 1 (or any other convenient gray level) correspond to objects, whereas pixels labeled 0 (or any other gray level not assigned to objects) correspond to the background. In general, a thresholding method is one that determines  $T$  based on a certain criterion. If  $T$  is determined solely from the gray level of each pixel, then the thresholding method is point-dependent. If  $T$  is determined from the local property (e.g., the local gray level distribution) in the neighborhood of each pixel, then the thresholding method is region-dependent. A global thresholding technique is one that thresholds the entire image with a single threshold value, whereas a local thresholding technique is one that partitions a given image into subimages and determines a threshold for each of these subimages.

The simplest of all thresholding techniques is to partition the image histogram by using a single global threshold. In an ideal case for a thresholding operator, the histogram is bimodal. That means that it has a deep and sharp valley between two peaks representing objects and background, respectively, so that the threshold can be chosen at the bottom of this valley [9]. However, for real pictures where the valley is flat and broad or when the two peaks are extremely unequal in height it is often difficult to detect the valley bottom precisely.

---

### 2.3.2 Otsu thresholding

---

This thresholding method, as proposed in [9], is based on the division of the pixels of an image into two classes  $C_0$ , and  $C_1$  (e.g., objects and background). The main goal is to maximize the separability of the resulting classes in gray levels.

Let us define two classes  $C_0 = (0, \dots, T)$  and  $C_1 = (T + 1, \dots, L - 1)$  with the threshold at level  $T$ . Let  $\sigma_W^2$ ,  $\sigma_B^2$ ,  $\sigma_{T0}^2$  be the within-class variance, between-class variance, and the total-variance, respectively.

The aim of maximizing the between-class variance can be achieved by maximizing one of the following and equivalent criterion functions:

$$\lambda = \frac{\sigma_B^2}{\sigma_W^2} \quad \eta = \frac{\sigma_B^2}{\sigma_{TO}^2} \quad \kappa = \frac{\sigma_{TO}^2}{\sigma_W^2} \quad (2.11)$$

This standpoint is based on the idea that a threshold with the best separation between classes in gray levels will be the optimal one. It is stated that  $\sigma_W^2$  and  $\sigma_B^2$  depends on threshold level  $T$ , but  $\sigma_{TO}^2$  is independent of it. It is also noticed that  $\sigma_W^2$  is based on the class variances or second-order statistics, while  $\sigma_B^2$  is based on the class means or first-order statistics. Therefore,  $\eta$  can be chosen as the simplest criterion measure with respect to  $T$  to evaluate the separability of the optimal threshold.

$$\eta(T) = \sigma_B^2 / \sigma_{TO}^2 \quad (2.12)$$

$$\sigma_B^2 = \frac{(\mu_{TO}\omega(T) - \mu(T))^2}{\omega(T)[1 - \omega(T)]} \quad (2.13)$$

where  $\omega(T)$  and  $\mu(T)$  are the zeroth- and the first-order cumulative moments of the histogram up to the  $T$ -th level and  $\mu_{TO}$  and  $p_l$  are the total mean level of the original image and the probability of level  $l$ , respectively.

$$\omega(T) = \sum_{l=0}^T p_l \quad \mu(T) = \sum_{l=0}^T l \cdot p_l \quad \mu_{TO} = \mu(L-1) = \sum_{l=0}^{L-1} l \cdot p_l \quad (2.14)$$

The optimal threshold  $T_{\text{opt, OT}}$  which can be restricted to cover just the effective range of a histogram will be selected by:

$$\sigma_B^2(T_{\text{opt, OT}}) = \max_{0 \leq T \leq L-1} \sigma_B^2(T) \quad (2.15)$$

This measure is consider significant due to its invariance under several transformations of the gray-level scale, such as for any shift or scale transformation.

---

### 2.3.3 Minimum error thresholding

---

Another method in thresholding presented in [8] is considering it as a classification problem, where the gray level distributions of object and background are known or can be estimated by the assumption of using a Gaussian distribution. In that way, using the results of statistical decision theory the optimal threshold will be achieved.

The standpoint of the minimum error thresholding method is to achieve a maximum efficiency in a criterion function related to the average pixel classification error rate.

Let us consider an image whose pixels assume gray level values,  $l$ , from the interval  $(0, L - 1)$ . According to [8] minimum error algorithm, the histogram  $h$  is viewed as an estimate of probability density function  $\hat{f}$  of the mixture population, which contains both object and background pixels. Considering a number  $i$  of classes, each of the two components of the mixture will be assumed to be normally distributed with a certain mean  $\mu_i$ , standard deviation  $\sigma_i$ , and a priori probability  $P_i$ . For these given

values, there will be a existing gray level  $l$  which has the Bayes minimum error threshold at which the image should be binarized. The problem is to determine the value of the certain threshold  $T_{\text{opt, ME}}$ .

The parameters  $\mu_i$ ,  $\sigma_i$ , and  $P_i$  of the mixture density  $\hat{f}$  will not be known, but they can be estimated from the gray level histogram  $h$ . To find the optimum threshold  $T_{\text{opt, ME}}$ , suppose that we threshold the gray level data at level  $T$  and model the objects and background populations by a normal density  $h(l|i, T)$  with parameters  $\mu_i(T)$ ,  $\sigma_i(T)$ , and  $P_i(T)$  given as:

$$P_i(T) = \sum_{l=a}^b h(l) \quad \mu_i(T) = [\sum_{l=a}^b h(l)l]/P_i(T) \quad (2.16)$$

and

$$\sigma_i^2(T) = [\sum_{l=a}^b \{l - \mu_i(T)\}^2 h(l)]/P_i(T) \quad (2.17)$$

where  $a$  and  $b$  are the two populations,

$$a = \begin{cases} 0 & \text{if } i = 1 \\ T + 1 & \text{if } i = 2 \end{cases} \quad b = \begin{cases} T & \text{if } i = 1 \\ L - 1 & \text{if } i = 2 \end{cases} \quad (2.18)$$

Using the models  $h(l|i, T)$ ,  $i=1,2$ , the conditional probability  $e(l, T)$  of gray level  $l$  being replaced in the image by a correct binary value, is:

$$e(l, T) = h(l|i, T) \cdot P_i(T)/h(l) \quad i = \begin{cases} 1 & \text{if } l \leq T \\ 2 & \text{if } l > T \end{cases} \quad (2.19)$$

From where we can get the quantity  $\epsilon(l, T)$  which can be considered as an alternative index of correct classification performance. Therefore, the image may be characterized by the criterion function:

$$J(T) = \sum_{l=0}^{L-1} h(l) \cdot \epsilon(l, T) \quad (2.20)$$

The amount of overlap presented between the Gaussian models of both object and background distributions will be subtly reflected by this criterion function. The threshold  $T$  will be varied along the histogram and the optimal threshold  $T_{\text{opt, ME}}$  will be found with the smaller overlap between density functions, which means a smaller classification error. According to that, the lowest value of criterion  $J(\epsilon, T)$  will give the minimum error threshold:

$$J(T_{\text{opt, ME}}) = \min_T J(T) \quad (2.21)$$

The criterion function has local minimum at the boundaries of the interval of gray levels. If the histogram is bimodal, there will be a unique and optimum internal minimum. In case of unimodal histograms, the absence of an internal minimum would lead to inappropriate binarisation. However, according to the authors in [8], this advocated method is in this case superior to Otsu which will produce 'salt and pepper' noise due to the fact of splitting the only mode in the middle. This method can also be extended to multithreshold selection.



---

### 2.3.4 Intermodos thresholding

---

For bimodal histogram images where objects and background can be clearly differentiated, the valley of the histogram can be chosen as the gray level threshold. The intermodes method, as can be seen in [10], is basically calculated by taking the first and second maximum peaks of the histogram and averaging them. To get these two peaks, the histogram is iteratively smoothed using a running average window of size 3, until there are only two local maximum:  $j_1$  and  $j_2$ . The optimal threshold  $T_{\text{opt, INT}}$  is then calculated as:

$$T_{\text{opt, INT}} = \frac{j_1 + j_2}{2} \quad (2.22)$$

As this method is really simple, it cannot be applied to images with extremely unequal peaks or to those with broad and flat valleys. Due to the fact that this thresholding is restricted to using a small smoothing window of three points for the histogram and that there are several limitations regarding to the use of histogram as an estimator, a variation of this procedure will be applied in the next section. This is related to the concept of Kernel Density Estimation as a smooth and optimal estimate of the pdf, and repeating again the fact of taking the two maximum peaks and averaging.

---

### 2.3.5 Limitations

---

As it has been said before, the histogram is a convenient tool for giving a graphical representation of a frequency distribution. Moreover, it is also one of the most widely used density estimators. However, it has some limitations that should be taken in mind.

Histograms are made up of bins and each bin represents a certain intensity value range. The histogram is computed by examining all the pixels of an image and assigning each pixel to a bin depending on its intensity. The final value of a bin is the number of pixels assigned to it. Generally, if the image is gray scale, 256 bins are used and if it is a binary image, two bins are enough to represent the intensity colors. If too few or too many bins are used, the histogram will be biased.

According to [7], the shape of the histogram depends on both the choice of the bin origin  $x_0$  and the bin-width, and making the wrong choice can lead to flawed interpretations. With too many bins, the structure of the data cannot be properly seen due to the presence of too much information. On the other hand, with too few there is no structure at all. Furthermore, the histogram is not a continuous function, and has jumps at the boundaries of the bins. It is not differentiable at the jumps and has zero derivatives elsewhere.

---

## 2.4 Kernel Density Estimation-based Thresholding

---

Using a kernel density estimator-based on thresholding, all those problems can be alleviated.

According to [7], kernel density estimators belong to a group class called non-parametric density estimators. They are characterized by requiring no prior information on the data model, whereas for parametric methods a priori information on the data model is needed.

Starting with the goal of removing the dependence on the end points of the bins, kernel estimators center a kernel function at each data point. If a smoothed kernel function is used for our building block, the result will have a smooth density estimate.

More formally said, kernel estimators smooth out the contribution of each observed data point over a local neighborhood of that data point. Assume a data vector  $\mathbf{r}$  with values between  $(1, \dots, L)$ . The contribution of data point  $r_l$  to the estimate at some point  $r$  depends on how apart these two points are. The scope of this contribution depends on both the shape of the adopted kernel function and the width accorded to it. Denoting the kernel function as  $K$  and its bandwidth by  $w$ , the estimated density at any point  $r$  can be defined as:

$$\hat{f}_w(r) = \frac{1}{L \cdot w} \sum_{l=1}^L K\left(\frac{r - r_l}{w}\right) \quad (2.23)$$

If we consider  $u = \left(\frac{r - r_l}{w}\right)$ , then  $\int K(u)du = 1$  to ensure the fact that the  $\hat{f}_w(r)$  integrates to 1.  $\hat{f}_w(r)$  can be written as the sum over the rescaled kernel functions. A graphical representation of this can be seen in Figure 2.5. The kernel function  $K$  can have different shapes (Uniform, Triangle, Epanechnikov, etc.). The Gaussian kernel function is the popular one.

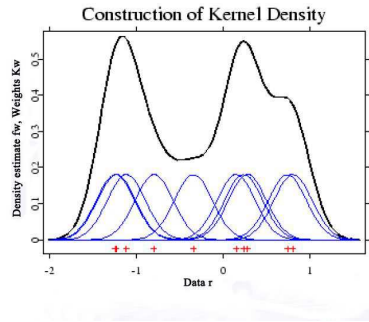


Figure 2.5: KDE,[7].

However, the problem of bin-width has not been tackled yet and the fact is that the quality of a kernel estimate depends less on the shape of  $K$  than on the value of its bandwidth  $w$ . In that way, there is a huge importance in the fact of choosing an appropriate bandwidth. Spiky estimates problems will be caused by small values and oversmoothing by larger ones.

In order to choose the optimal bandwidth, a common method is used. Its standpoint is motivated by the idea of using the bandwidth value that minimizes the AMISE (Asymptotic Mean Integrated Squared Error). This can be obtained as an approximation of the formula MISE (Mean Integrated Square Error).

$$\text{MISE}(\hat{f}_w) = \text{mean} \left[ \int_{-\infty}^{+\infty} \{\hat{f}_w(x) - f(x)\}^2 dx \right] = \int \text{MSE}\{\hat{f}_w(x)\} dx \quad (2.24)$$

$$w_{\text{opt}} = \arg_{\min}(\text{AMISE}) \quad (2.25)$$

In that way, it is needed to estimate the AMISE from our data so that the chosen bandwidth will be an asymptotic approximation. This specific choice of bandwidth collects all the important features whilst maintaining smoothness. All these ideas can be extended to multiple dimensions.

In this thesis, the estimated probability density function is used together with an intermodes extension of finding the optimal threshold by looking to the two maximums and averaging them. In that way, the optimal threshold for KDE,  $T_{\text{opt, KDE}}$ , will be also calculated as:

$$T_{\text{opt, KDE}} = \frac{j_1 + j_2}{2} \quad (2.26)$$

## 2.5 Watershed Segmentation

### 2.5.1 Watershed principle

According to [5], concept of watershed segmentation can be developed by visualizing an image  $I(x, y)$  in three dimensions. Comparing a gray-level image with a topographic relief (two spatial coordinates:  $x, y$ ) where the altitude corresponds to the gray level of a pixel, valleys corresponding to the dark parts and hills corresponding to the bright areas will be found. In Figure 2.6, this topographic relief can be seen applied to our test strip device.

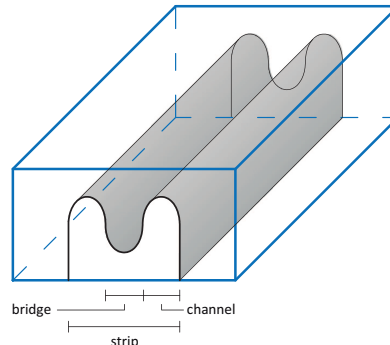


**Figure 2.6:** Watershed segmentation example.

The main goal of this segmentation algorithm can be ideally achieved by punching holes in each regional minimum of the image and flooding the entire topography from below by letting water rise through the holes with uniformity. If distinct catchment basins are about to merge because of the rising water, a dam or watershed line is built to prevent the merging. Finally, only the tops of the dams will be visible above the water line. By extracting these boundaries, the segmented image is obtained.

One of the main applications of watershed segmentation is the extraction of nearly uniform objects from a certain background. Regions with small variations in gray levels have small gradient values. In these cases, watershed segmentation is often applied to the gradient of the image where the edges can clearly be found.

---

## 2.5.2 Dam Construction

---

Dam construction is applied to binary images, and the simplest way to construct them is to use morphological dilation. They are used to separate a catchment basin from another, in case that the rising water threatens to merge them.

Suppose  $q$  is an element of a set  $Q$  of connected components at the  $n$ th step and  $C(n - 1)$  the set flooded catchment at step  $n - 1$ , then the dams are constructed by dilating  $q \cap C(n - 1)$  with a  $3 \times 3$  structuring element of 1's. However, the dilation is performed under two conditions. The first condition is that it is constrained by  $q$ , and the second one is that the dilation cannot be performed on points that would cause the sets being dilated to merge.

---

## 2.5.3 Watershed Segmentation Algorithm

---

Considering an image  $I(x, y)$ , its segmentation involves dividing it into  $R$  non-empty connected sets  $M_1, M_2, \dots, M_R$  with the coordinates of the points in the regional minimum of the image.

Before denoting the image, the possible different points need to be defined. According to [5], when a drop of water falls on a topological surface, it could belong to: first a regional minimum; second, to a single minimum (catchment basins will be created) and third, to more than one region (they will form watershed lines). Starting from  $n = \min + 1$  integer increments to  $n = \max + 1$ , the topography will be flooded, where  $\min$  and  $\max$  are the minimum and maximum values of  $I(x, y)$ . By using only values of  $n$  that correspond to existing gray-level values in  $I(x, y)$ , the efficiency can be improved.

Following, the union of all flooded catchment basins is denoted by:

$$C(\max + 1) = \bigcup_{i=1}^R C(M_i) \quad (2.27)$$

where  $C(M_i)$  is the set of coordinates of points in the catchment basin  $C$  associated with the regional minimum  $M_i$  that are being flooded.

---

## 2.5.4 The Use of Markers

---

Due to the fact that an automatic application of the watershed algorithm to the gradient image involves oversegmentation problems which can make results practically useless because of noise and other irregularities, the use of markers is introduced.

The definition of a marker is a connected component belonging to an image. By creating both internal and external markers, extra information of the interesting objects and background can be obtained. This priori knowledge is relevant to the segmentation problem which can improve it.

For our test strip measurements, by creating internal and external markers, we can get more information about the ROI. These markers are given by an Otsu thresholding. The external markers are given by threshold  $T_{R, \text{MAX}}$  that describes the regional maximum of the image, which corresponds to the test strip. And the internal markers are given by  $T_{R, \text{MIN}}$  that determines the regional minimum, which includes the information inside the strip: bridge and channels. For  $T_{R, \text{MAX}}$  and  $T_{R, \text{MIN}}$ :

$$T_{R, \text{MAX}} > T_{R, \text{MIN}} \quad (2.28)$$

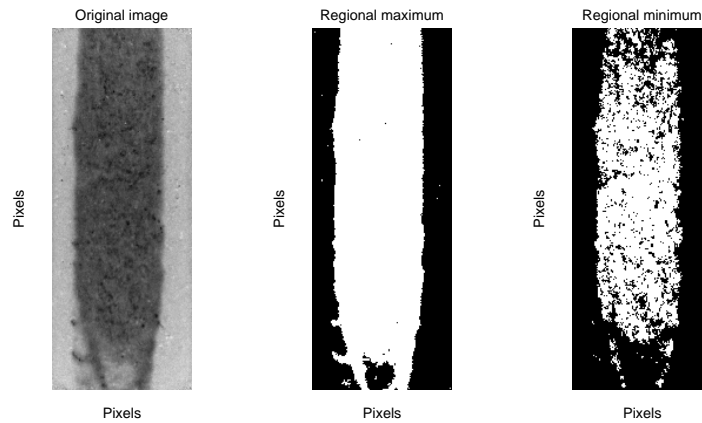


**Figure 2.7:** Regional maximum and Regional minimum for a 550mg/dL example.

### 2.5.5 The Distance Transform

A widespread method used in association with the watershed transform is the Distance Transform. According to [6], it is applied to binary images and it marks the distance from every pixel to the nearest non-zero value. To compute this distance, the common method is the Euclidean distance.

It mainly reduces the effect of oversegmentation due to the fact that in a distance edge map, the main boundaries of the original image are visible, whereas noise or small details are not evident. That avoids its confusion with possible dams presented in the original image.

For our test measurements, the distance transform is calculated on the external markers of the image. In that way, we are labelling each of its pixels with the distance to the nearest boundary pixel of the image. Consecutively, the gradient is calculated in order to smooth more detail inside the strip and get less oversegmentation. Moreover, by imposing the internal markers, we enlarge the difference between object and background, what help to improve the segmentation.

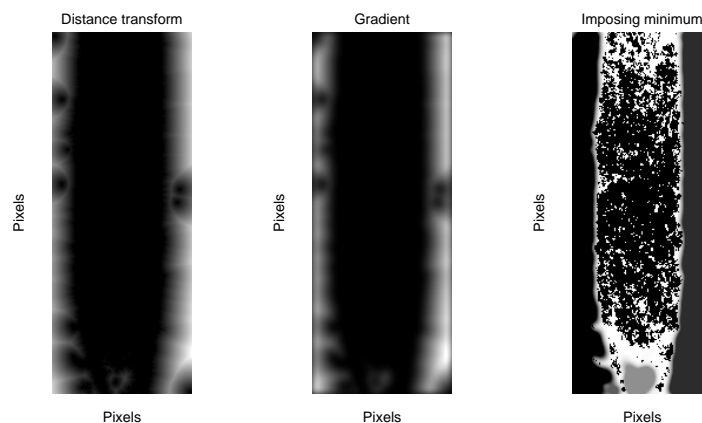


**Figure 2.8:** Distance transform, gradient and the imposed minimums for a 550mg/dL example.

Finally, the watershed segmentation is calculated of the smoothed gradient image with the imposed minimum points. The condition for the regional maximum to be zero is imposed and the image labelled.

The connected component with bigger area of the image will give the segmentation of the channels of the test strip.

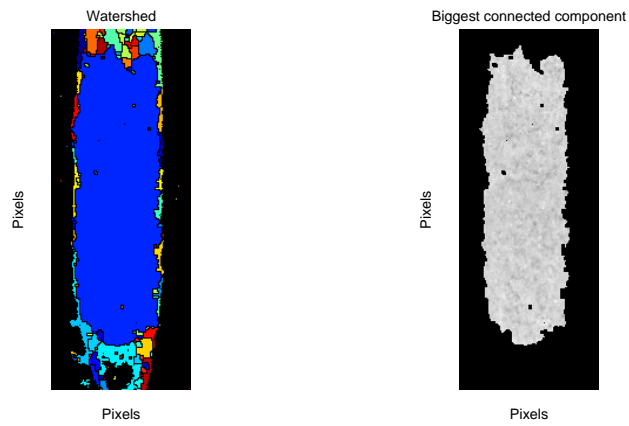


**Figure 2.9:** Watershed segmentation and biggest connected component for a 550mg/dL example.

## 3 Data Set

This chapter introduces the real data sets. The idea is to show what they represent and the different artifacts that can degrade them.

### 3.1 Test Setup

As mentioned in Section 1, a test setup has been created, where the chemical reaction of a blood sample is monitored using a set of sensors that result in an image during approximately 20s. This is equivalent to 607 images/set. We have 44 different sets corresponding to 5 different blood glucose levels.

In each of the sets, we can clearly differentiate between the frames we observe in Figure 3.1. These frames are the following:

- **Frame 1:** Dark image. This image represents the internal side of the device without the test strip and without the lights.
- **Frame 2:** Light image. This image represents the internal side of the device without the test strip but illuminated.
- **Frame 3-6:** Dark images. These show the device area without illumination and serves as a calibration subset.
- **Frame 7-31:** Light images. These show the device area with illumination and with the test strip in the device, but before the blood sample is detected. They also serve as calibration images.
- **Frame 32- 607:** The blood sample is detected and the glucose reaction takes place.

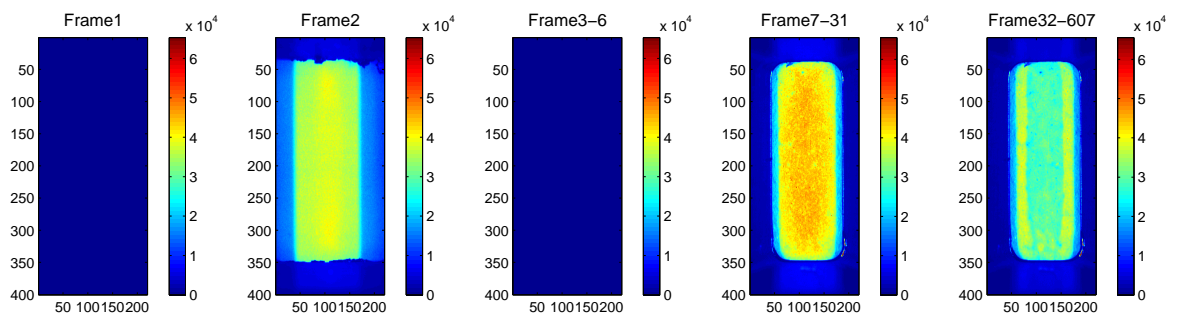


Figure 3.1: Different frames of a particular blood glucose frames.

However, the intensities values of the different sets cannot be compared. They need all to have the same normalized intensity values. Because of that, we will start looking at the relative remission estimation values,  $\widehat{rR}$ . This concept is clearly explained in the following quotient:

$$\widehat{rR} = \frac{\text{reflected light of the current frame}}{\text{reflected light of the normalization frames}} \quad (3.1)$$

By this way, all values become independent from the LEDs lighting, and we can proceed to compare the different sets. The normalization frames are calculated by using Frames 3-31.

### 3.2 Artifacts

The images recorded by the camera can be degraded by different artifacts that appear in them, such as noise, dust or air bubbles. These can either appear for a certain time interval and disappear or can be present through all the entire measurement. Moreover, the proposed algorithm should not only be able of detecting artifacts but also should be robust against shift movements of the test strip. An example of both a dust particle and an air bubble particle are shown in Figure 3.3, where we can see both the original image and the algorithm mask. Clearly, the mask manages to identify the artifacts and the algorithm does not consider this area in the estimation process.

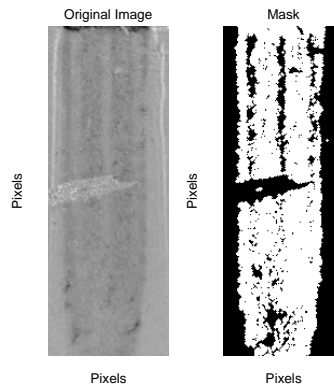


Figure 3.2: Dust artifact.

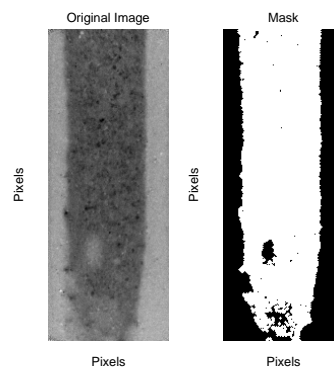


Figure 3.3: Air bubble artifact.



# 4 Proposed Algorithm and Evaluation

This chapter explains the different functions developed in our algorithm and gives an evaluation to the different methods that have been used. A flow graph of the approach can be seen in Figure 4.1.

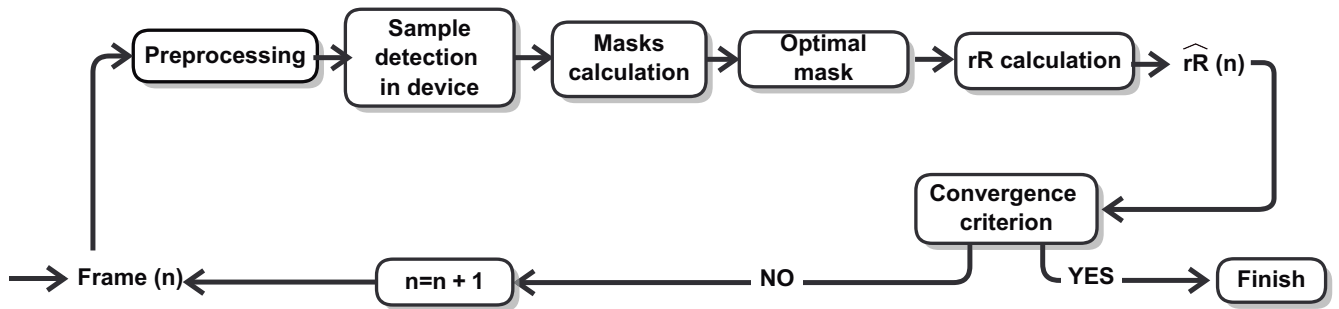


Figure 4.1: General idea of the proposed algorithm.

## 4.1 Preprocessing

According to the flow graph presented in the Figure 4.3, there are two main operations:

### 1. Crop:

As we are only interested in the evaluation area where the blood sample has been placed, we proceed to crop the image. The difference between the cropped and the original image can be seen in Figure 4.2. This will decrease the size of the image, hereby decreasing the execution time. It also gets rid of irrelevant information in the image.

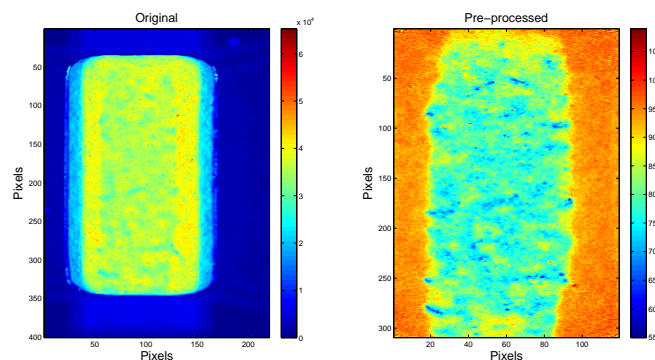


Figure 4.2: Example of cropped and original frame.

The final cropped frame will have different dimensions depending on the maximum intensity value of the image. To calculate the cropped image dimensions, we take a reference image before the

frame where the blood sample is detected by the device, which will give us information about the intensity borders of the strip, as well as its concrete position and a threshold between (0,...,1) to specify how much we want to crop the image. Considering  $m$  the image maximum intensity and  $T_{\text{crop}}$  the threshold specified, we get:

$$T_{\text{opt, crop}} = m \cdot T_{\text{crop}} \quad (4.1)$$

If a pixel of the image has a smaller value than the  $T_{\text{crop}}$  then it gets a zero value. According to that, the low intensity borders are removed, and if the strip is not completely inside the device, the remaining empty area is also removed. Consequently, the dimensions of the image do not depend on the glucose level but on initial conditions of the current image. However, these dimensions are approximately the same due to the fact that the test strip area is usually of equal size in the images.

## 2. Normalize:

After cropping, we calculate the average of the 'empty light' and 'empty dark' frames, taking as a consequence (Frames 3-6), (Frames 7-31) from Section 3.1, respectively. Considering  $I_{\text{light}}$  the average empty light and  $I_{\text{dark}}$  the average empty dark, we get:

$$I_{\text{light}} = \frac{\sum_{k=7}^{31} I_k}{25} \quad I_{\text{dark}} = \frac{\sum_{k=3}^6 I_k}{4} \quad (4.2)$$

To normalize the frames and get the relative remission values, we proceed to work with both the difference and the division operators.

First of all, we work with the difference between the initial dark frame and  $I_{\text{dark}}$  to make sure we have a black image at the beginning. And secondly, work with the difference between the average empty light frames and the average empty dark frames we have just calculated. This is the flat intensity area with the strongest reflection.

$$I_{\text{flat}} = \frac{I_{\text{light}} - I_{\text{dark}}}{100} \quad (4.3)$$

Secondly, we work with the division between the 'current' frame and the flat intensity area. The new values of the normalized frames,  $I_{\text{norm}}$ , can be called relative remission and they are always between 0 and 100. Value 100 is the strongest reflection and denotes the initial value before the reaction has taken place. The relative remission value will decrease more the higher the glucose value is.

$$I_{\text{norm}} = \frac{I_{\text{current}} - I_{\text{dark}}}{I_{\text{flat}}} \quad (4.4)$$

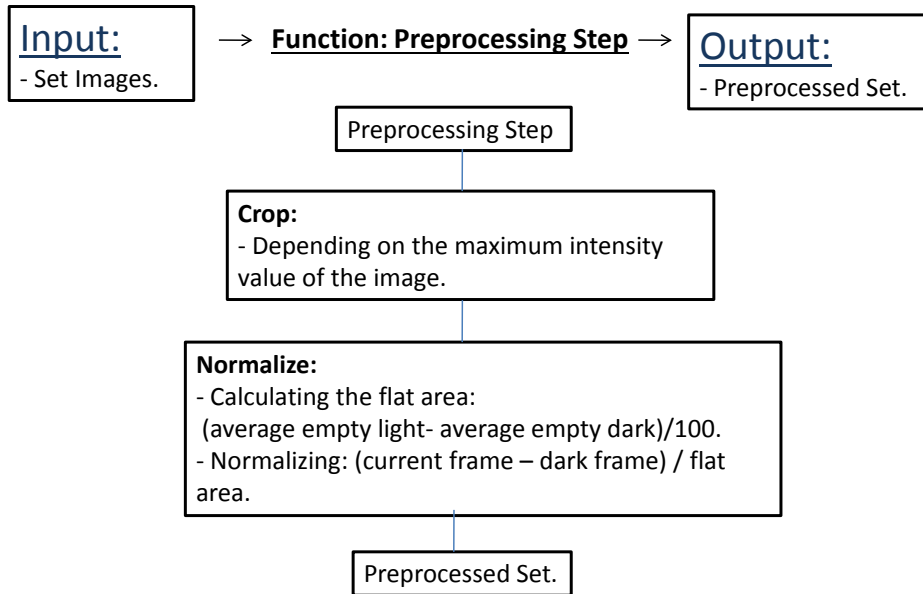


**Figure 4.3:** Preprocessing Step.

## 4.2 Sample detection in device

This step, as we can see in Figure 4.5, deals with the fact of detecting which is the frame when the blood sample placed on the test strip is detected by the device. To accomplish it, we proceed to work with the mean of the absolute difference between two consecutive frames,  $m$ . Considering  $M \cdot N$  the total number of pixels and  $k$  the number of frames, we get:

$$m(k) = \frac{1}{M \cdot N} \sum_{i=1}^N \sum_{j=1}^M |I_k(i, j) - I_{k+1}(i, j)| \quad (4.5)$$

The maximum value will give us the position of this frame. However, it should be taken into account that the blood sample needs a few milliseconds to be completely detected by the device. Because of that, we add to the maximum value an offset of five frames, which is equal to 150ms.

$$SID = \max(m) + \text{offset} \quad (4.6)$$

The graph in Figure 4.4 shows the absolute difference between consecutive frames for set 30 mg/dL. The SID frame is usually detected around frame 72, which is equal to 2.4 seconds.

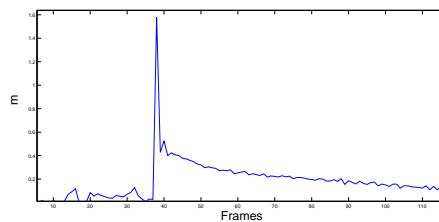


**Figure 4.4:** SID Graph.

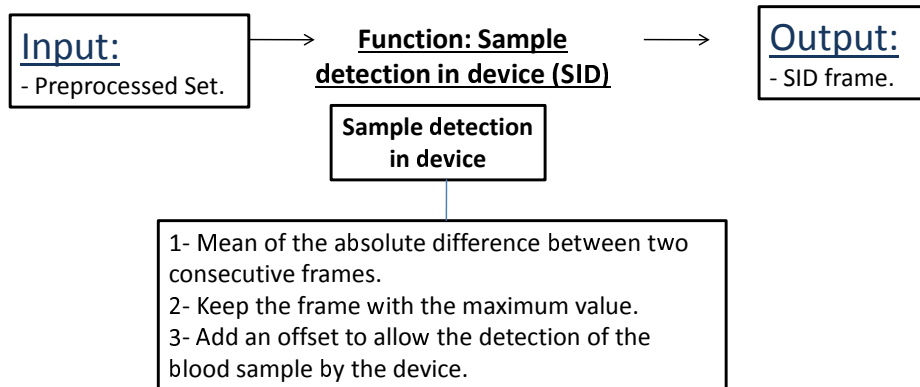


**Figure 4.5:** Sample in the device.

### 4.3 Masks calculation

The main objective is now to segment the blood sample from its background. To achieve this goal, we proceed to observe the histogram of the different sets of images. They are depicted in Figure 4.6.

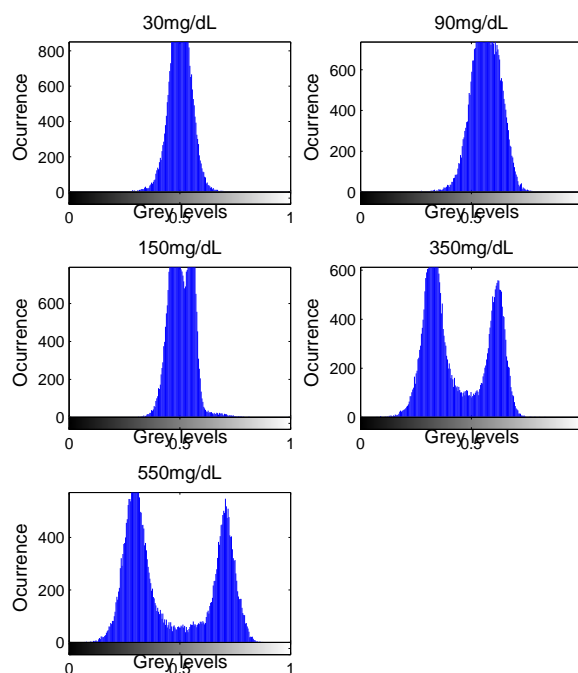


**Figure 4.6:** Histogram of exemplary images taken from different glucose values.

Due to the strong color reaction of higher level glucose, we can clearly differentiate two peaks in its histogram (bimodal). However, the small color reaction that appears in lower levels glucose histograms makes it more difficult to differentiate between the strip and the ROI considering that it only has one peak. Therefore, for lower glucose values we need an extra preprocessing step to estimate the value accurately.

---

This preprocessing consists on giving contrast to the frame with a logarithmic transformation and applying a median filter to it. This filter is useful for eliminating salt and pepper noise, typical of the image. The idea is to achieve a bimodal histogram and proceed to threshold it, as in higher levels glucose (Section 2.2). After that, an opening operator is also applied so as to clean the image from more noisy particles. However, this new preprocessed frame is also limited by the low glucose small color reaction during the whole set of images, what implies the impossibility of detecting neither the channels nor the bridge of the test strip. However, according to that, the SID frame, calculated in the previous function, it is considered to be enough in order to get at least the area where the test strip is situated.

To sum up, in the following steps, this algorithm is based on the calculation of two masks:

- The first mask, also called SID mask, always represents the frame when the blood sample is detected by the device. A contrast logarithmic function is applied to it.
- The second mask, also called TIME mask, changes over the time representing the whole frames of the test measurement.

One of the SID mask utility is that it is able of detecting the existing artifacts that are presented on the test images during the whole measurement. However, it represents a solid structure of the test strip with no detail on it. The TIME mask, once the color reaction has taken place, is be able of giving a better mask. Depending on the strength of the color reaction, it may differentiate between the channels and the test strip. For that reason, the SID mask will be specifically used for low glucose levels. Moreover, both of them make the algorithm to be robust against test strip movements due to the fact that the masks will change place according to the test strip location in the image.

Furthermore, for achieving the appropriate masks calculation we have the choice between different based-thresholding methods. These are Otsu thresholding (OT), Minimum error thresholding (ME), Intermodos (INT) and Kernel density estimator-based thresholding (KDE), all of them mentioned in Section 2.3. In this thesis, the normalized images we are working with have intensity values between (0 – 100). We are working with 256 bins and it can be said that the precision of all threshold images is enough. Moreover, the watershed segmentation method is used as an extension to Intermodos thresholding and provides a further alternative.

$$\text{ROI} = \text{optimal mask} \cdot \text{original image} \quad (4.7)$$

---

#### 4.3.1 Evaluation of thresholding-based and segmentation methods

---

Otsu Thresholding (OT) method does not take into account any probability distribution, what makes it capable of giving in every moment a correct optimal mask: SID mask for lower glucose values, where the frame mask is unimodal, and the TIME mask for higher glucose values.

If we look in detail to Minimum Error Thresholding (ME) for example in 150 mg/dL, it can be seen that even the SID frame threshold, which comes from a bimodal histogram, is not a good result. As we can see in the histogram of Figure 4.8, the original image belongs to an image that has not a Gaussian behavior and presents a large tail due to a light particle presented on the image. According to that, the optimal threshold calculated is not in the middle of both populations and the binarization is incorrect. This does not happen in the Otsu thresholding due to the fact that it does not take into account any probability

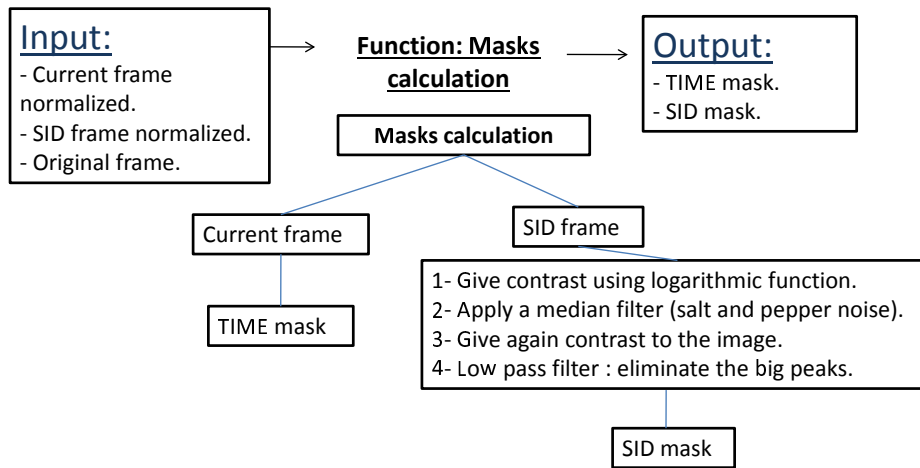


Figure 4.7: Masks calculation.

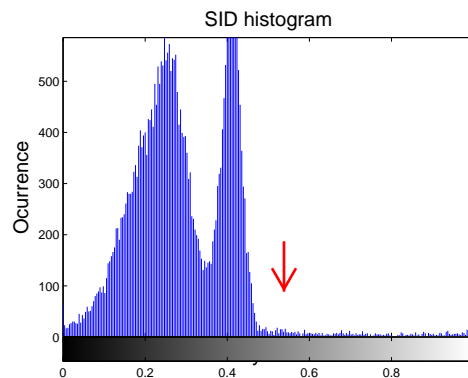


Figure 4.8: Problematic histogram for ME thresholding.

distribution, and in that way, the value that maximizes the separability of the resultant classes is the accurate one.

If we look in detail to Intermodos Thresholding (INT), we see the same error as with ME: the chosen threshold of the SID histogram is incorrect. For higher glucose levels, the smoothing step gets two differentiated peaks corresponding to both objects and background presented in Figure 4.9. However in lower glucose values, although we are working with the SID frame, the bimodal histogram typically reflects two unequal peaks as we can see in Figure 4.10. The fact of having unequal peaks makes one of them go unnoticed during the smoothing step, taking as second maximum a peak presented in the noise tail. Different sizes for the smoothing window have been tried, but still there is not a good thresholding. The extension of part of the Intermodos Thresholding method to Kernel Density Estimation (KDE) solves this problem. In this way, KDE calculates a smooth estimate of the probability density function and after that, the two maximum peaks are calculated. The final  $T_{opt, KDE}$  is obtained by averaging them, as we can see in Figure 4.11.

To sum up, as we can see in Figure 4.12, Otsu method and KDE method provide better results than the others taking into account lower glucose values (SID mask). Dealing with these two methods in depth, we can see how for higher values they obtain similar results in Figures 7.4 and 7.5. For lower values and depending on the unimodality, both methods can either give a good result without applying contrast to the image or not. The advantage of Otsu against KDE can be seen in the sets of 150 mg/dL,

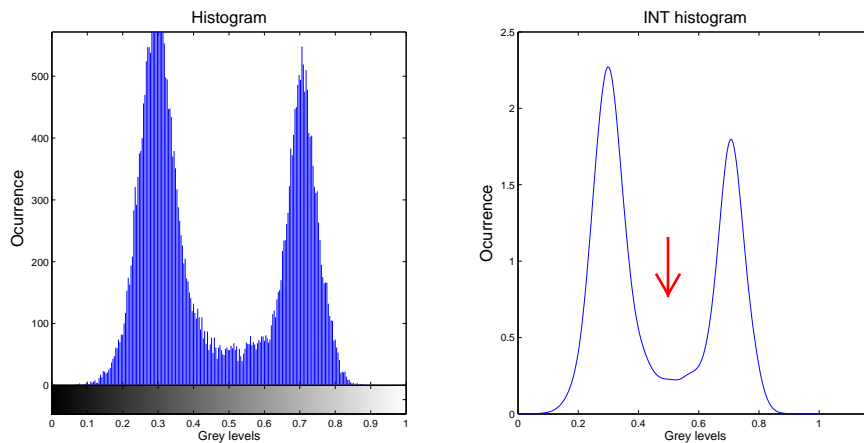


Figure 4.9: Histogram INT. Thresholding for a 550mg/dL frame.

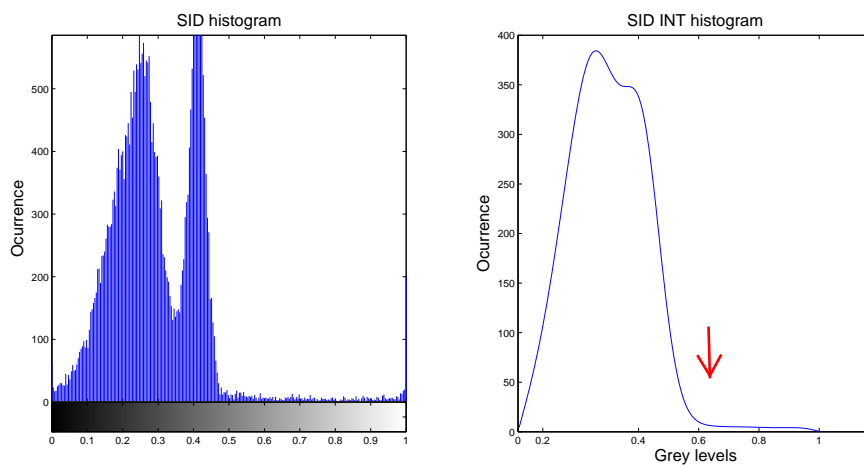


Figure 4.10: Histogram INT. Thresholding for a 150 mg/dL SID frame.

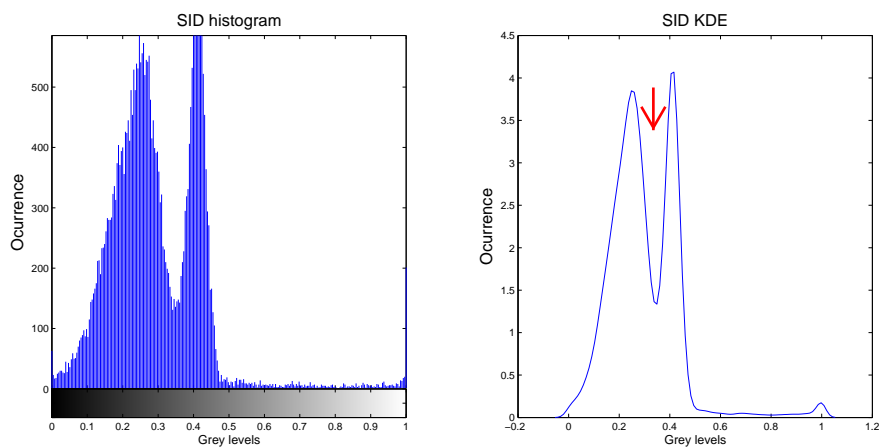
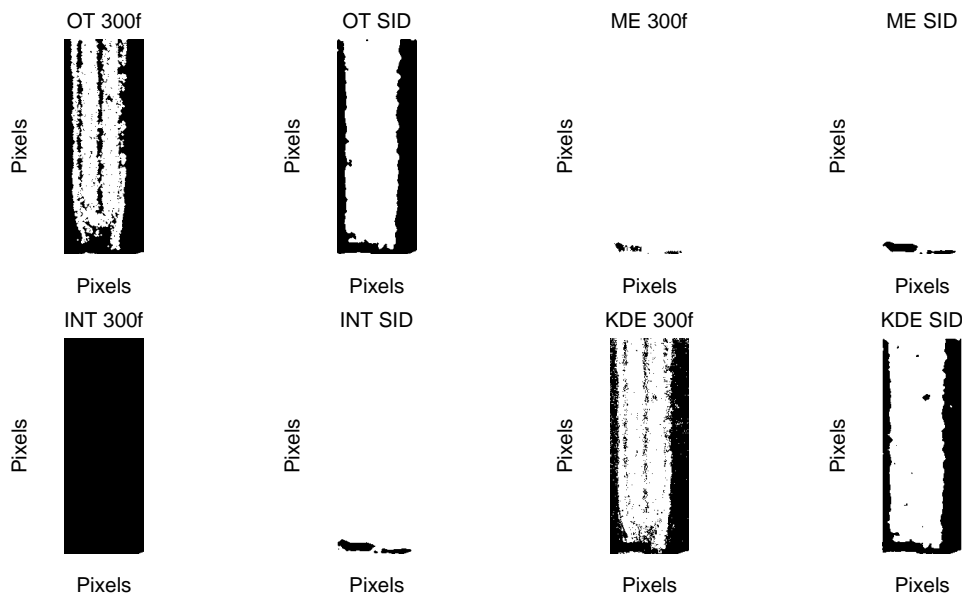
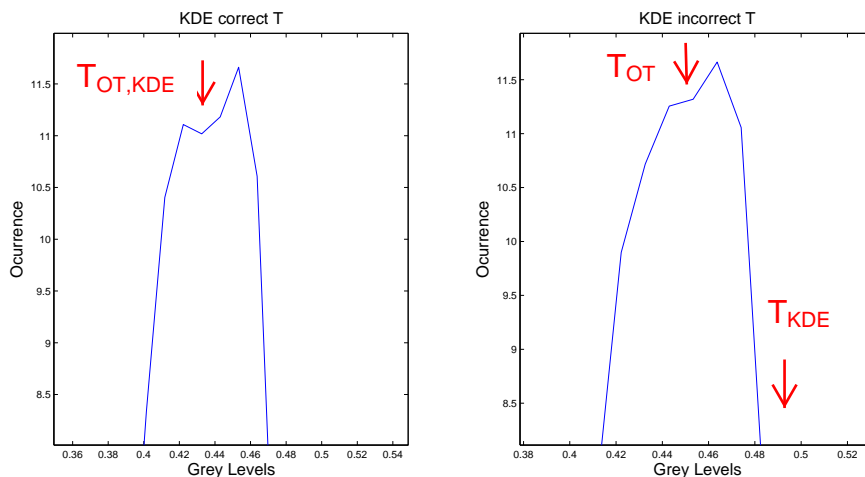


Figure 4.11: Histogram KDE. Thresholding for a 150 mg/dL SID frame.

for example in Figure 4.13, where both images have a good thresholding with Otsu method, but only one (left image) has a good thresholding with KDE. In the right image, one of the classes goes unnoticed because it does not achieve a maximum in the estimated probability function. However, the maximum separability between classes detects it.



**Figure 4.12:** Mask from the different thresholding methods: 150 mg/dL.



**Figure 4.13:** Correct and incorrect thresholding of KDE for two different frames.

With regard to watershed segmentation, it gives good results in high glucose values, by giving more information of the ROI due to the use of internal and external markers. By applying it to the smoothed gradient with the regional minimum imposed, we detect air bubbles and small particles that can have influence on the estimation of the relative remission value. This can be seen in Figure 4.14. However, when the internal markers return a good result by segmenting both the channels and the bridge, the watershed segmentation procedure produces an over-segmentation of the ROI making difficult the fact of detecting it. These cases can be seen in Figure 4.16.



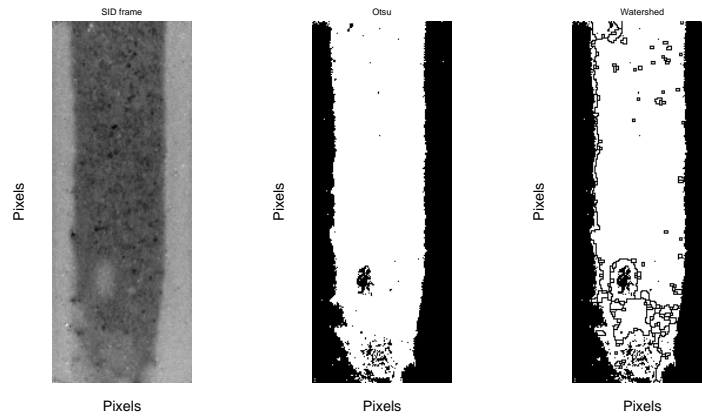


**Figure 4.14:** Watershed segmentation for high glucose values.

Moreover, the main problems of watershed segmentation are presented in low glucose values. When the original frame does not show a strong color reaction and the SID frame is taken into account. In this case, as we can see in Figure 4.15, this method gives an over-segmentation of the inside part of the strip that has not much sense, due to the fact, that even the internal markers of the thresholded image are not able of detecting neither the channels nor the bridge of the strip.

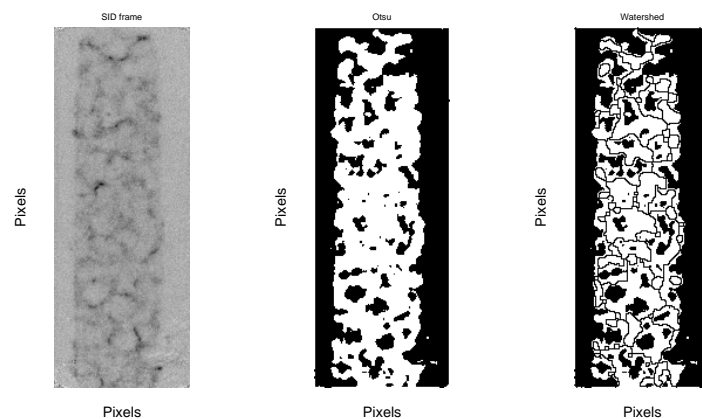


**Figure 4.15:** Watershed segmentation for low glucose levels.

Further on, we will focus the results to OT thresholding, KDE-based thresholding and watershed segmentation.

#### 4.4 Optimal Mask

In order to be able to assess the superiority of a certain mask, we take into account two main characteristics:

- **Black borders of the image:** According to the image dimensions and taking into account possible noise of the image, we give an extra opening operator to the obtained mask before counting the number of black columns presented on the image. In this calculation, a 5% of the top and bottom image is not taken into account due to the fact that there usually remains noise that belongs to

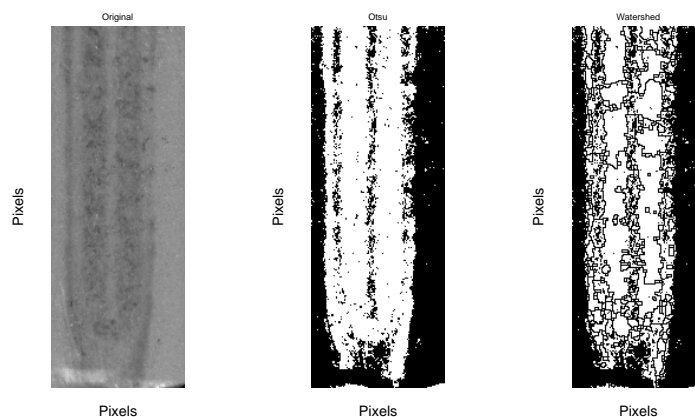


**Figure 4.16:** Watershed segmentation for high glucose levels.

the test strip. The presence of thicker borders (bigger number of columns) will be a condition to know if the mask has been calculated correctly. We can see that this condition remains even in the original test strip structure that we can see in Figure 1.3. An example of the black borders of a mask is presented in Figure 4.17.

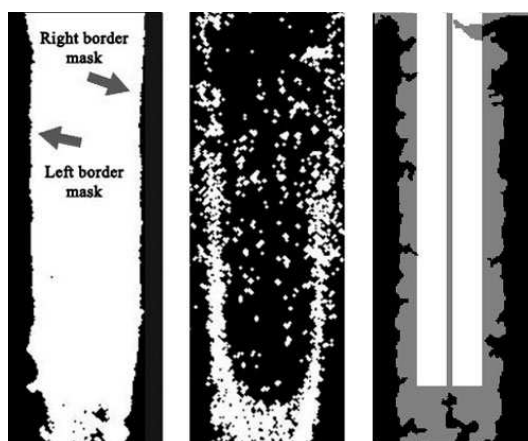


**Figure 4.17:** Optimal mask (550mg/dL), non-optimal mask(30mg/dL) and minimized SID mask.

- **Number of black pixels of an image:** According to the strip field measurements, we can claim that the black area of the mask should not exceed a certain value of the image dimensions. This is a safety condition so that the whole image is not black.

Finally, we multiply this mask by the original image and its relative remission value will be estimated by taking the mean of the area.

#### 4.5 Relative remission calculation

Before calculating the relative remission values,  $\widehat{rR}$ , a minimum size of the ROI is required to be able to get a reliable estimate. This requirement was given by Roche Diagnostics. In that way, we check the number of white pixels that correspond to the obtained optimal mask. If the number of white pixels of the optimal mask is bigger than the minimum value, the  $\widehat{rR}$  will be calculated.

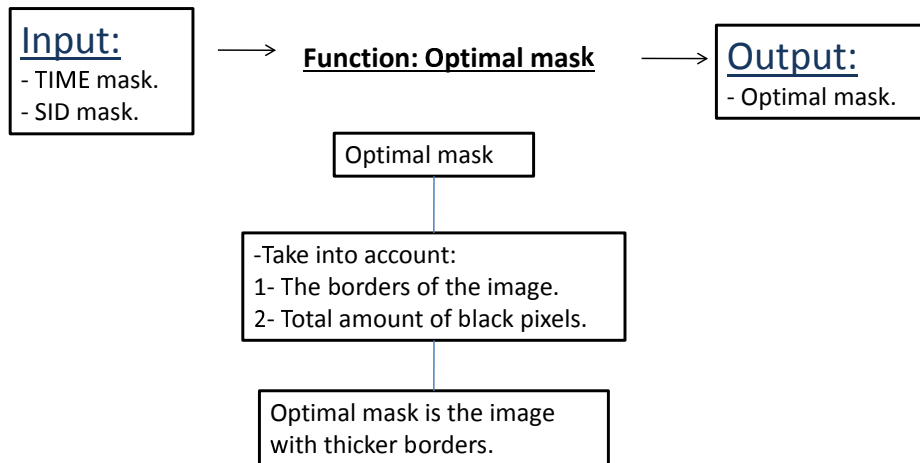


**Figure 4.18:** Optimal mask.

Typically, the SID mask is larger than the channel region, where the blood sample is situated. According to that, in case of using it for lower glucose values, we proceed to minimize its area according to the size of the channels, as we can see in Figure 4.17. The starting point for the SID mask to be reduced is the center of its biggest connected component.

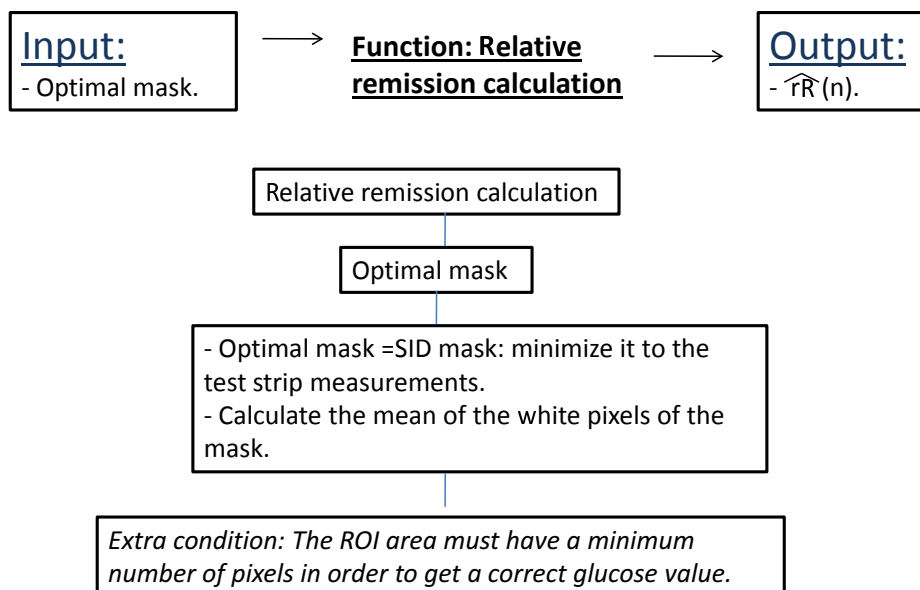


**Figure 4.19:** Relative remission calculation.

## 4.6 Convergence criterion

Once we have the  $\hat{rR}$  of the first three frames, we start looking to the convergence frame. As we have mentioned in Section 1, Roche Diagnostics defines the convergence to take place when the inter-frame difference is equal or smaller than 1% for three consecutive times in a row. It should be also taken into account that, in previous frames to the SID the blood sample has not been detected yet, so we should look after this period of time.

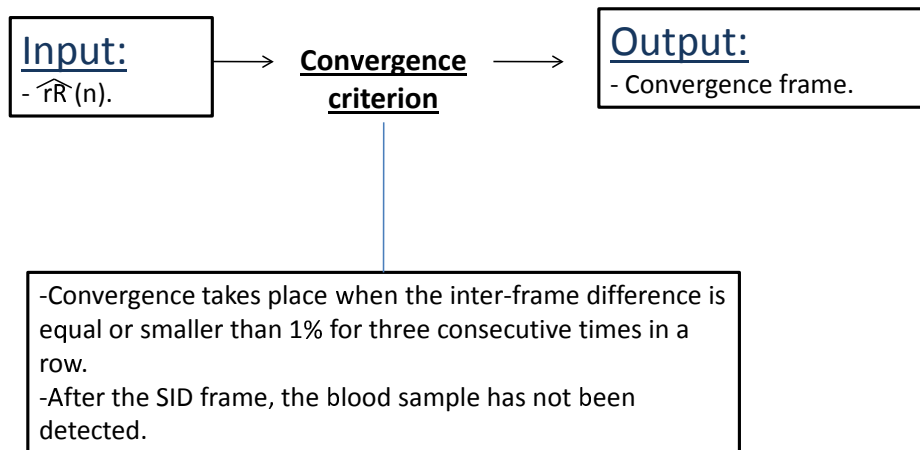


**Figure 4.20:** Convergence criterion.

---

# 5 Experimental Results

This chapter examines the different results of the proposed algorithm. We have tested our methods using a real data set of 44 measurements, described in Section 3.

---

## 5.1 Otsu thresholding method

---

In this section, we present from Table 5.1 to 5.5 the convergence frame and convergence time calculated with the respective relative remission values for each of the glucose levels. For 30 mg/dL, the values start to converge sooner due to the small color reaction that takes place in the test strip. According to each of the glucose levels the mean of the convergence time can be seen, in Table 5.8. In Figure 5.2 we can see a graph with the respective relative remission estimation of all glucose levels. If we compare it with the ideal Kinetic curve, presented in Figure 1.4 of Section 1, we can see the expected time behavior. Lower glucose values are related to higher  $\widehat{rR}$  whereas higher glucose values are related to lower ones. In Figure 5.1 we can see another representation of the relative remission values with regard to the glucose levels.

The variance of the relative remission values and the mean of the computation time of the algorithm are presented in Table 5.6. The variance of each glucose levels present low values, what means that the function works uniformly for all sets regardless of if they have artifacts or not. For example, the test measurement number 1 from 150 mg/dL presents the dust artifact mentioned in Subsection 3.2, and the behavior of this convergence frame is the same in a subsection. For the glucose value 90 mg/dL we find the biggest variance value. This can be owing to the fact that in lower glucose values the algorithm uses the SID frame, which has less accuracy. The fact of having in 30 mg/dL the smallest variance value, is not because the SID frame has more accuracy, but because the 30 mg/dL frames are more homogeneous. With regard to the computation time, we can say that they have low values.

Furthermore, we can check the superiority of calculating the TIME mask with a certain method for higher glucose values. In Table 5.7, we present the  $\widehat{rR}$  for the convergence frame of higher glucose values obtained by applying the SID mask during the whole test measurement. In that way, we avoid the optimal mask step and we directly calculate the ROI estimation. It can be seen that the  $\sigma_{\widehat{rR}}^2$  values have increased for all of them.

---

## 5.2 Kernel density estimation-based thresholding method

---

In this section, we present from Table 5.9 to 5.13 the convergence frame and convergence time calculated with its respective relative remission value for each of the glucose levels. In Table 5.11, we can see how two of the test measurements do not detect a convergence frame. This can be explained by looking to Figure 5.4, where some of the kinetic curves for 150mg/dL do not converge by representing a constant variation of the relative remission values. As explained in Chapter 5, this is due to the fact that the threshold is not always correctly calculated, and there is a small variation depending on choosing the SID mask or the TIME mask. For the other glucose levels the mean of the convergence time can be seen,

Test measurements	Convergence Frame	Convergence Time(s)	$\widehat{rR}$
1	155	5.10	97.13
2	185	6.09	97.62
3	232	7.64	97.22
4	168	5.53	97.43
5	155	5.10	97.13
6	168	5.53	97.92
7	156	5.14	97.57
8	161	5.30	96.75

**Table 5.1:** Otsu method: 30 mg/dL.

Test measurements	Convergence Frame	Convergence Time(s)	$\widehat{rR}$
1	366	12.05	86.75
2	446	14.69	85.48
3	367	12.09	86.31
4	518	17.06	84.06
5	500	16.47	85.41
6	454	14.95	84.43
7	417	13.73	85.14
8	389	12.81	86.32
9	413	13.60	88.99

**Table 5.2:** Otsu method: 90 mg/dL.

Test measurements	Convergence Frame	Convergence Time(s)	$\widehat{rR}$
1	436	14.36	78.98
2	463	15.25	77.45
3	525	17.29	79.38
4	428	14.10	78.81
5	437	14.39	78.60
6	435	14.33	78.80
7	363	11.96	79.23
8	413	13.60	79.23
9	565	18.61	76.27

**Table 5.3:** Otsu method: 150 mg/dL.

Test measurements	Convergence Frame	Convergence Time(s)	$\widehat{rR}$
1	397	13.08	65.70
2	404	13.31	65.94
3	450	14.82	64.89
4	388	12.78	66.11
5	464	15.22	63.97
6	390	12.85	65.16
7	444	14.62	64.61
8	448	14.76	63.65
9	404	13.31	65.51

**Table 5.4:** Otsu method: 350 mg/dL.

Test measurements	Convergence Frame	Convergence Time(s)	$\widehat{rR}$
1	413	13.60	58.76
2	404	13.31	58.39
3	378	12.45	58.61
4	344	11.33	59.40
5	413	13.60	57.88
6	372	12.25	59.41
7	364	11.99	60.43
8	367	12.09	59.39
9	461	15.18	59.47

**Table 5.5:** Otsu method: 550 mg/dL.

Glucose value	30	90	150	350	550
$\sigma^2_{\widehat{rR}}$	0.13	1.99	1.04	0.65	0.56
Computation Time (s/frame)	0.24	0.29	0.28	0.27	0.32

**Table 5.6:** Otsu method: variance and computation time of the  $\widehat{rR}$ .

Glucose value	150	350	550
$\sigma^2_{\widehat{rR}}$ TIME mask	1.04	0.65	0.56
$\sigma^2_{\widehat{rR}}$ SID mask	1.07	0.92	0.74

**Table 5.7:** TIME mask and SID mask of the  $\widehat{rR}$  for high glucose levels.

Glucose value	30	90	150	350	550
Convergence Time (s)	5.67	14.16	14.87	13.86	12.86

**Table 5.8:** Otsu method: mean of the convergence time for each glucose value.

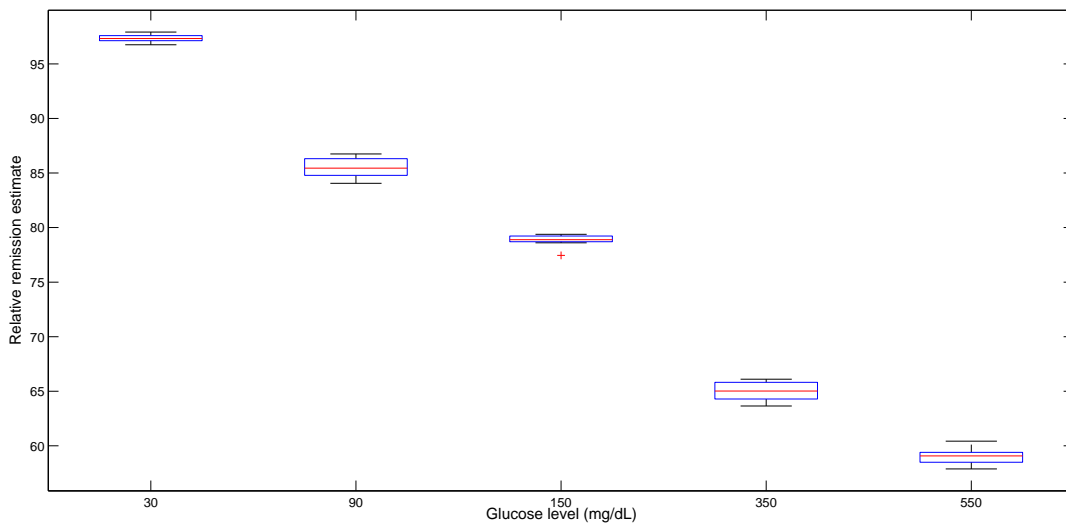


**Figure 5.1:**  $\widehat{rR}$  for all glucose levels with Otsu.

Test measurements	Convergence Frame	Convergence Time(s)	$\widehat{rR}$
1	155	5.10	97.11
2	184	6.06	97.64
3	202	6.65	97.51
4	163	5.37	97.47
5	156	5.14	97.06
6	164	5.40	97.89
7	156	5.14	97.52
8	161	5.30	96.74

**Table 5.9:** KDE method: 30 mg/dL.

in Table 5.15. In Figure 5.3 we can see another representation of the relative remission values with regard to the glucose levels, and in this case, we can see how for 150mg/dL, the  $\widehat{rR}$  contains a bigger range of values.

The variance of the relative remission values and the mean of the computation time of the algorithm are presented in Table 5.14. The variance of 150mg/dL is the double as the variance in Otsu method, due to its no convergence Kinetic curve. But for 30 and 90 mg/dL, where the SID mask is used to achieve bimodality, the estimate density function plays a huge role to detects the peaks correctly. Generally, all the computation time values have increased, specially the critical glucose level of 150mg/dL.

### 5.3 Watershed segmentation method

In this section, we present the results of the watershed segmentation method. From Table 5.16 to 5.18 we can see the number of the convergence frame and convergence time calculated with its respective



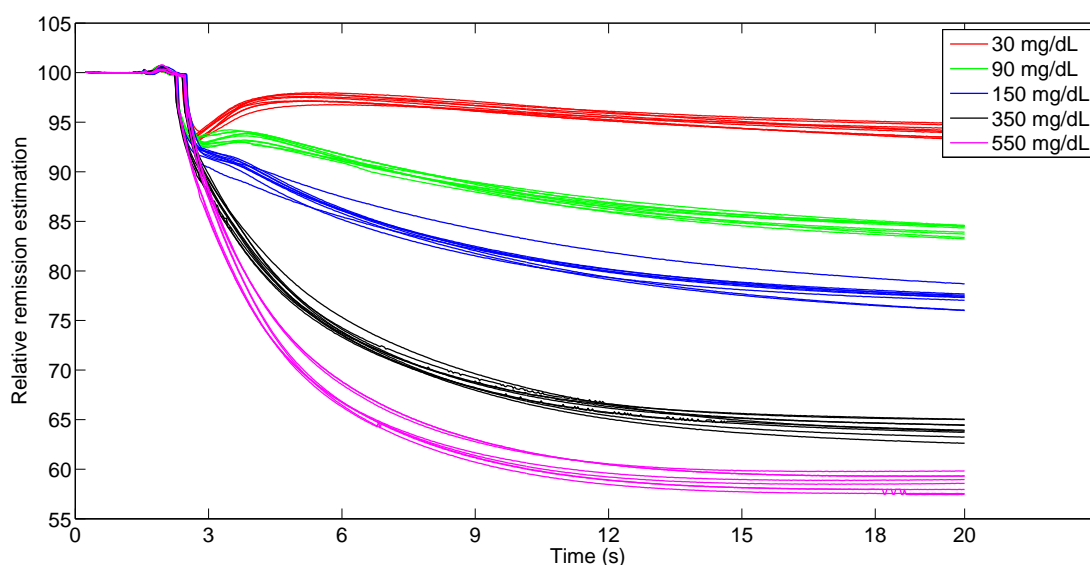


Figure 5.2: OTSU Kinetik curve for all glucose levels.

Test measurements	Convergence Frame	Convergence Time(s)	$\widehat{rR}$
1	425	14.00	86.11
2	433	14.26	85.61
3	367	12.09	86.31
4	518	17.06	86.10
5	406	13.37	86.14
6	476	15.68	84.80
7	427	14.06	84.96
8	389	12.81	86.32
9	413	13.60	85.02

Table 5.10: KDE method: 90 mg/dL.

Test measurements	Convergence Frame	Convergence Time(s)	$\widehat{rR}$
1	566	18.64	77.67
2	469	15.45	77.24
3	-	-	-
4	-	-	-
5	395	13.01	78.48
6	384	12.65	79.18
7	363	11.96	79.23
8	264	8.69	81.63
9	441	14.50	77.15

Table 5.11: KDE method: 150 mg/dL.

Test measurements	Convergence Frame	Convergence Time(s)	$\widehat{rR}$
1	357	11.56	66.89
2	358	11.75	66.57
3	479	15.78	64.38
4	418	13.77	64.96
5	423	13.93	64.34
6	423	13.93	65.45
7	444	14.62	64.54
8	393	12.94	64.36
9	404	13.31	65.50

**Table 5.12:** KDE method: 350 mg/dL.

Test measurements	Convergence Frame	Convergence Time(s)	$\widehat{rR}$
1	413	13.60	58.78
2	397	13.08	58.49
3	378	12.45	58.61
4	404	13.31	58.89
5	413	13.60	58.01
6	373	12.29	59.45
7	364	11.95	60.07
8	367	12.09	59.52
9	461	15.18	59.49

**Table 5.13:** KDE method: 550 mg/dL.

Glucose value	30	90	150	350	550
$\sigma^2_{\widehat{rR}}$	0.13	0.38	2.55	0.93	0.41
Computation Time (s/frame)	0.29	0.30	0.46	0.33	0.41

**Table 5.14:** KDE method: variance and computation time of the  $\widehat{rR}$ .

Glucose value	30	90	150	350	550
Convergence Time (s)	5.52	14.10	13.55	13.53	13.04

**Table 5.15:** KDE method: Mean of the convergence time for each glucose value.

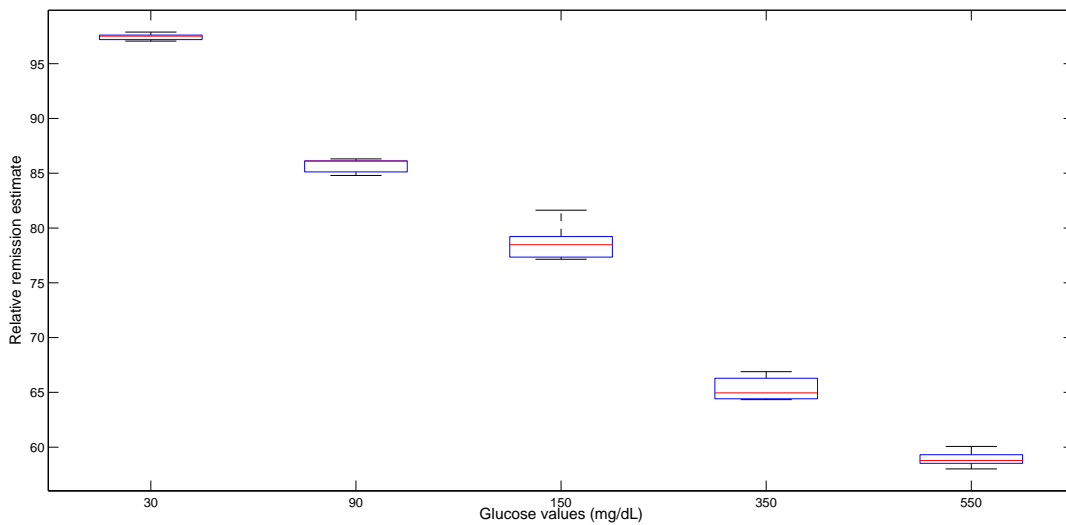


**Figure 5.3:**  $\widehat{rR}$  for all glucose levels with KDE.

Test measurements	Convergence Frame	Convergence Time(s)	$\widehat{rR}$
1	436	14.36	78.91
2	476	15.68	77.23
3	525	17.29	79.33
4	428	14.10	78.31
5	389	12.81	79.11
6	419	13.80	79.01
7	363	11.96	79.11
8	413	13.60	79.18
9	496	16.34	77.04

**Table 5.16:** Watershed segmentation: 150 mg/dL.

relative remission value for high glucose levels, where the watershed segmentation results can be worthwhile. For both 350 and 550 mg/dL we found two cases where the convergence frame has not been found. This is because the convergence condition has not taken place due to the fact that the difference of the relative remission values between consecutive frames is larger than 1%. This value depends on the particular procedure, so in this case different details are found inside the test strip from one frame to another.

The variance of the relative remission values and the mean of the computation time of the algorithm are presented in Table 5.19. We can see that for 150mg/dL the variance is lower, whereas for 350mg/dL and 550mg/dL the variance is higher with regard to the Otsu Method. Bear in mind that the computation time depends on the set dimensions we get after applying the crop function, we can say that this method takes much more time than the Otsu method. In Figure 5.5 we can see another representation of the relative remission values with regard to the glucose levels from 150mg/dL to 550mg/dL.

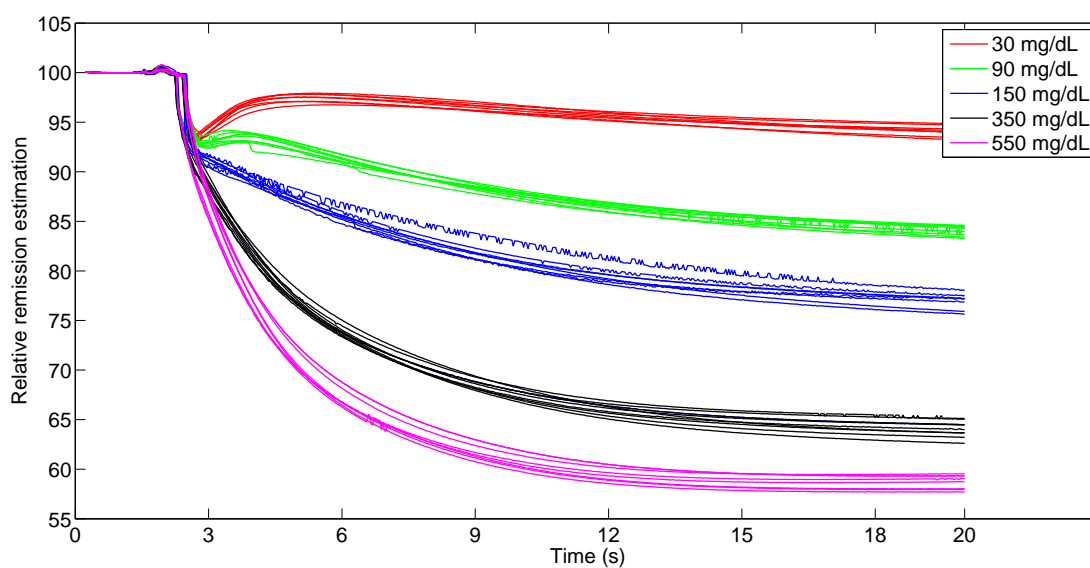


Figure 5.4: KDE Kinetik curve for all glucose levels.

Test measurements	Convergence Frame	Convergence Time(s)	$\widehat{rR}$
1	439	14.46	65.06
2	423	13.93	65.76
3	500	16.47	64.19
4	403	13.27	65.89
5	243	8.00	68.81
6	410	13.50	65.11
7	-	-	-
8	466	15.35	62.99
9	-	-	-

Table 5.17: Watershed segmentation: 350 mg/dL.

Test measurements	Convergence Frame	Convergence Time(s)	$\widehat{rR}$
1	413	13.60	58.76
2	404	13.31	57.83
3	595	19.60	57.96
4	344	11.33	59.27
5	464	15.28	57.76
6	358	11.79	59.37
7	-	-	-
8	368	12.12	59.30
9	-	-	-

Table 5.18: Watershed segmentation: 550 mg/dL.

Glucose value	150	350	550
$\sigma^2_{\widehat{rR}}$	0.75	2.7	1.4
Time (s/frame)	0.31	0.53	0.79

**Table 5.19:** Watershed segmentation: variance and computation time of the  $\widehat{rR}$ .

Glucose value	150	350	550
Convergence Time (s)	14.43	13.56	13.86

**Table 5.20:** Watershed segmentation: Mean of the convergence time for each glucose value.

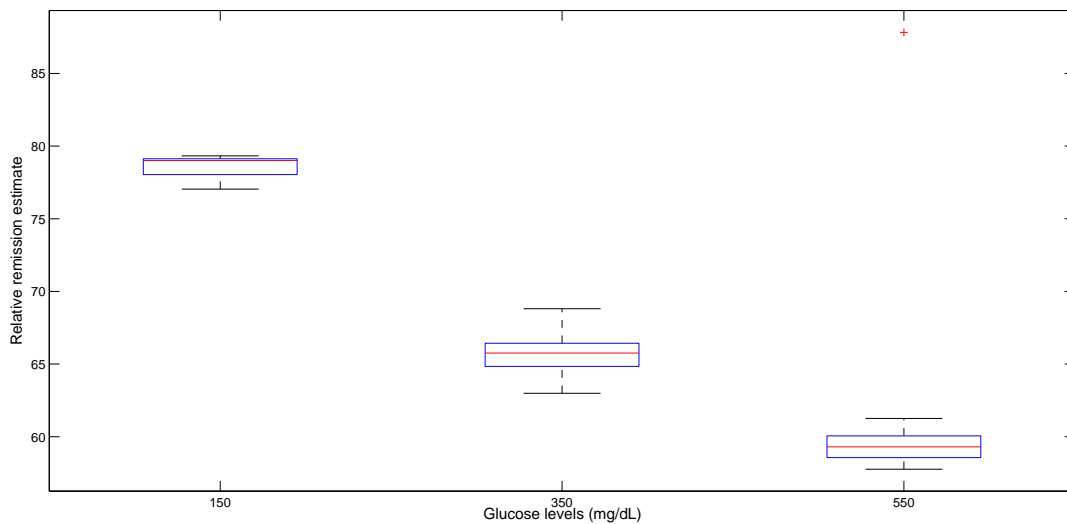


**Figure 5.5:**  $\widehat{rR}$  for all glucose levels with Watershed segmentation.

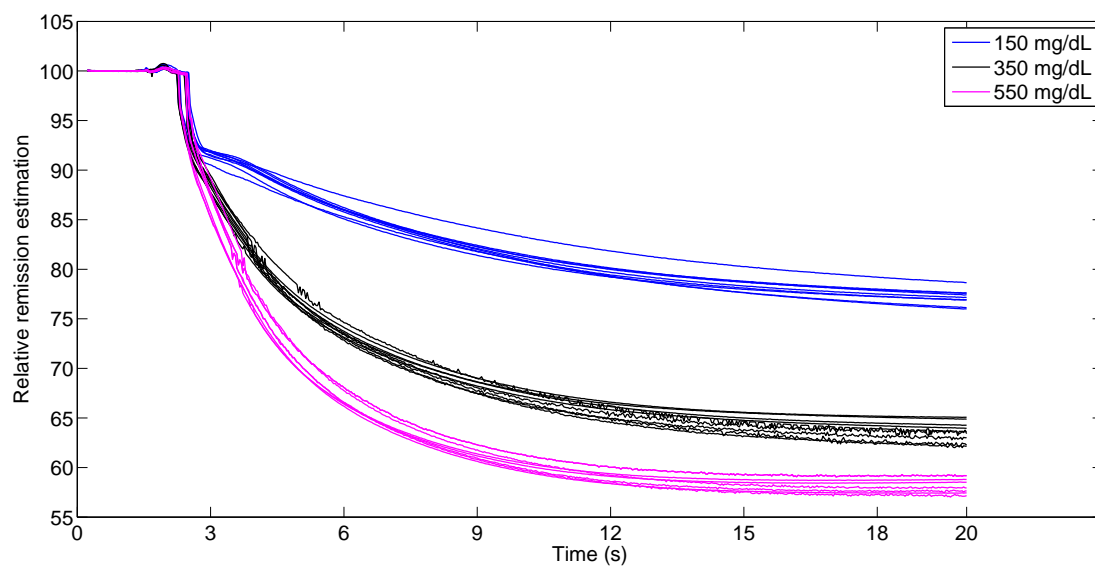


**Figure 5.6:** Watershed segmentation Kinetik curve for all glucose levels.

---

## 6 Conclusion and Outlook

In this thesis, a segmentation algorithm for measuring blood glucose in hand-held devices is discussed. The proposed algorithm is basically based on histograms thresholding using different methods and watershed segmentation in order to obtain the ROI. Afterwards, the mean of the area is taken as an estimate. It is formulated in Matlab.

The methodology makes the theoretical part of the thesis and gives an overview of the different methods and operators utilized in the proposed algorithm. The procedure presented first includes image preprocessing, what involves both cropping and normalizing the image in order to work with the area we are interested in and at the same time being able of comparing all these values. Secondly, the detection of the frame when the blood sample is detected by the device (SID frame). After that, several thresholding methods are used, such as Otsu thresholding, minimum error thresholding, intermodes and its extension using Kernel density estimation. Finally watershed segmentation is also used. For lower glucose cases, the masks produced by thresholding SID frames proved to be better, as it works with unimodal histograms by applying a contrast transformation to it. Finally, a relative remission estimation of the blood sample is calculated. One important property of this algorithm is the low computation time needed to estimate the relative remission estimation.

One goal of this work was to analyze several thresholding methods, such as Otsu method, minimum error thresholding, intermodes and its extension using kernel density estimation. Otsu method and kernel density estimation-based thresholding proved to provide better results, due to the fact that they do not take into account any probability distribution, and they are not limited to equal peaks on the estimated density function. Another goal of this work was to preprocess the data sets before applying watershed segmentation. However, these combination appears to slow down the algorithm and its results are not worthwhile enough. This is mainly due to oversegmentation problems, despite the fact of using both markers and the distance transform methods.

Furthermore, a convergence criterion is applied by looking to the time behavior of the relative remission estimation. In that way, the convergence frame is obtained and its value is compared to the other test measurements.

Further work might uses other kind of combinations with regard to the different methods, in order to achieve more accuracy in the optimal mask calculated, specially with regard to low glucose values where the SID mask presented is not accurate enough to take the relative remission estimation.

# 7 Annex

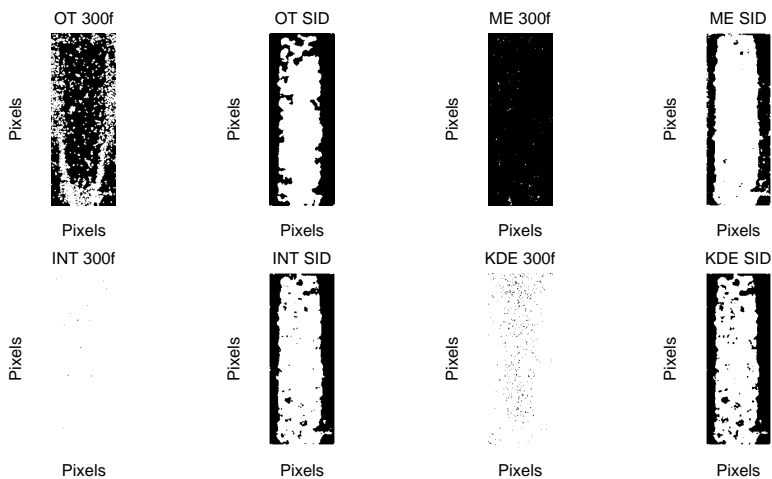


Figure 7.1: Mask from the different thresholding methods: 30 mg/dL.

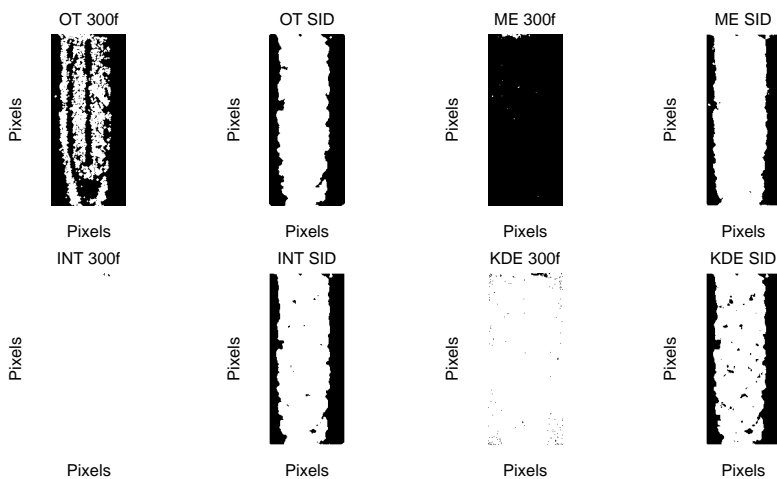


Figure 7.2: Mask from the different thresholding methods: 90 mg/dL.



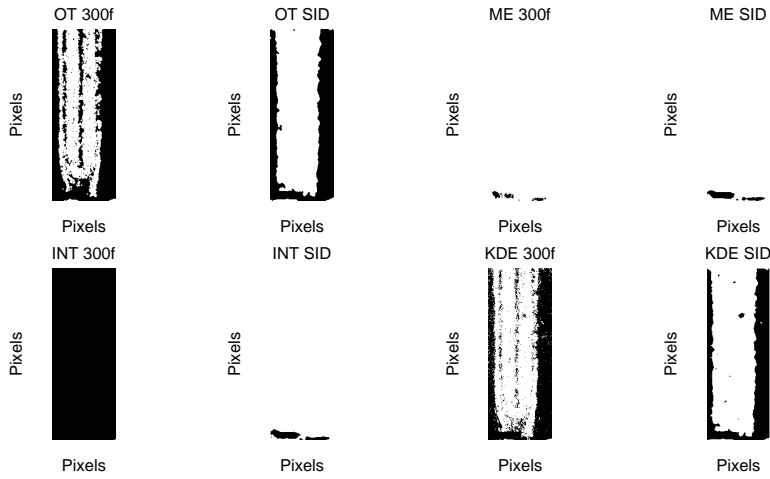


Figure 7.3: Mask from the different thresholding methods: 150 mg/dL.

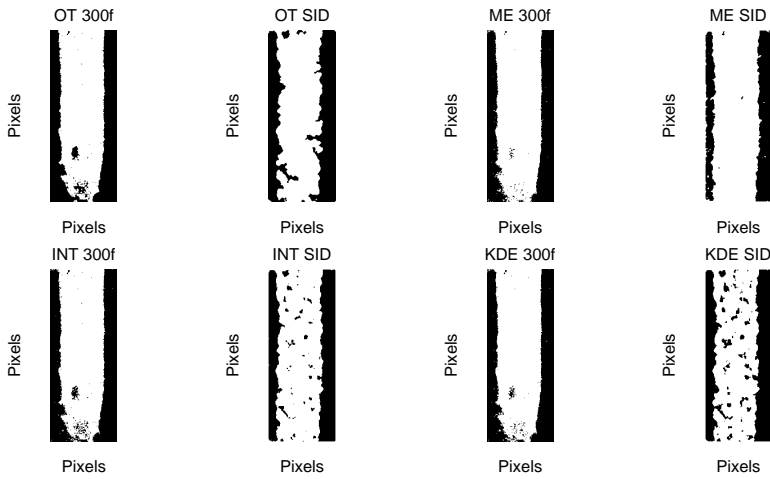


Figure 7.4: Mask from the different thresholding methods: 350 mg/dL.

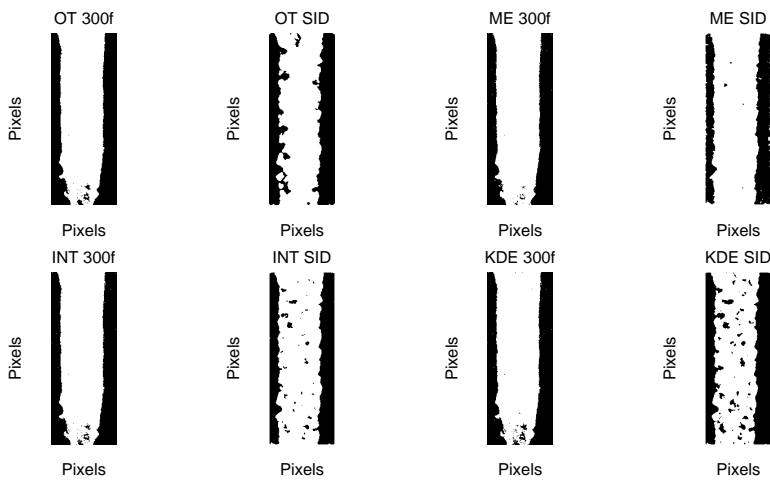
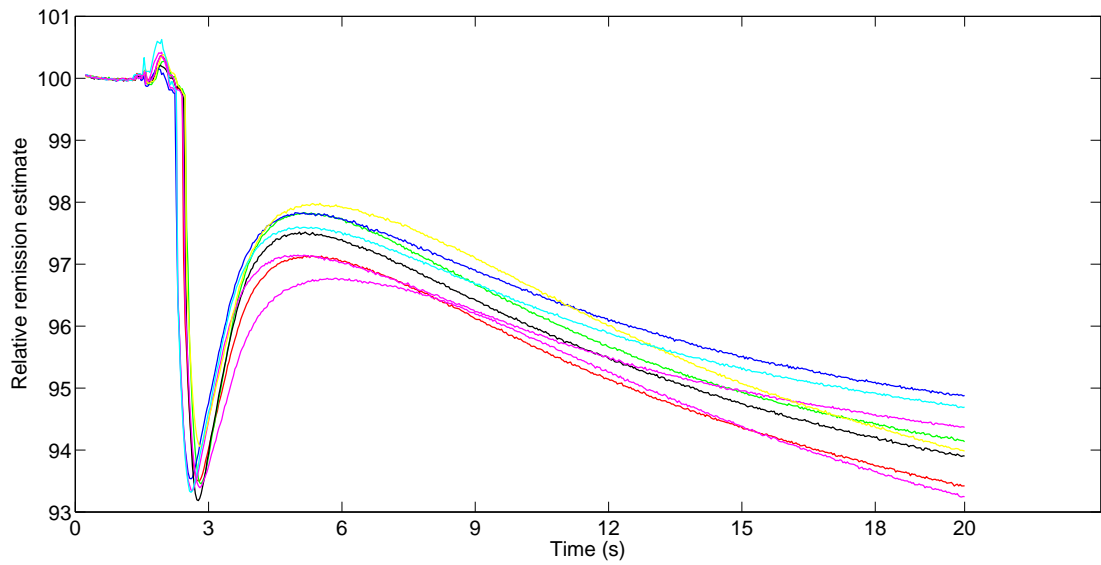
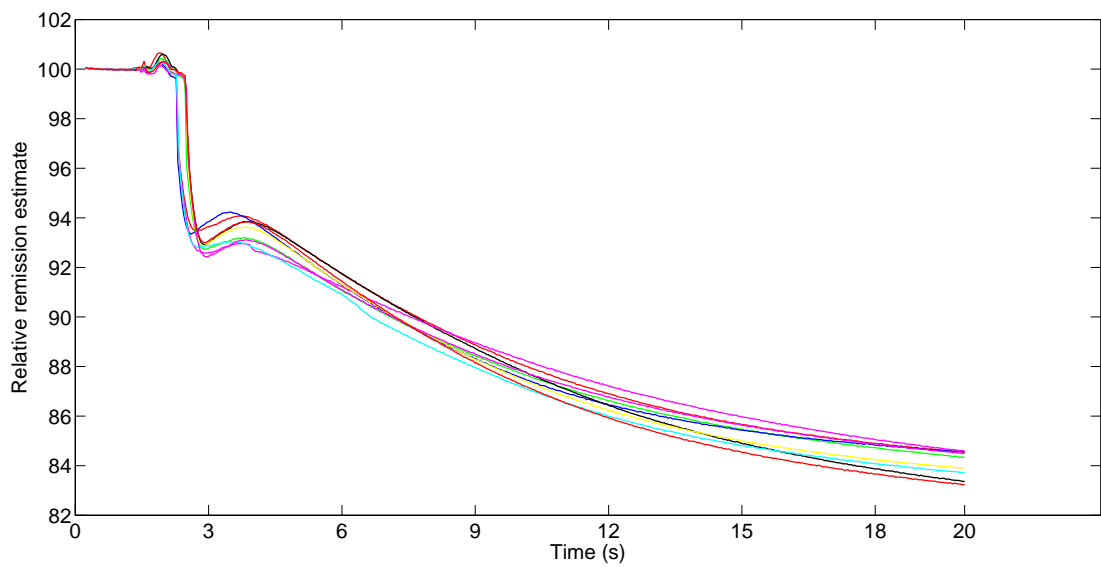


Figure 7.5: Mask from the different thresholding methods: 550 mg/dL.



**Figure 7.6:** OTSU Kinetik curve 30 mg/dL.



**Figure 7.7:** OTSU Kinetik curve 90 mg/dL.

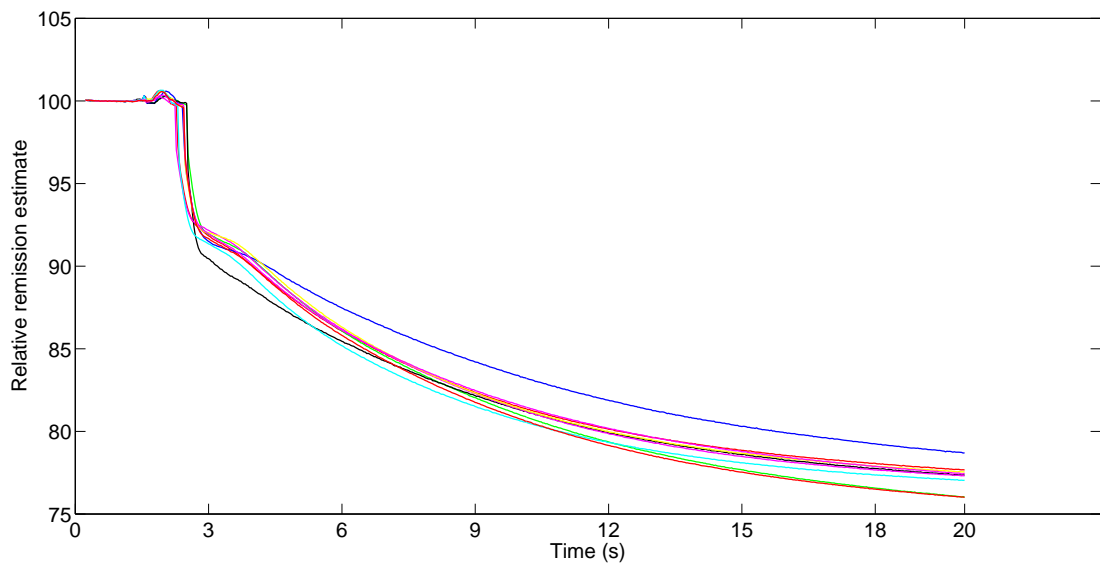


**Figure 7.8:** OTSU Kinetik curve 150 mg/dL.

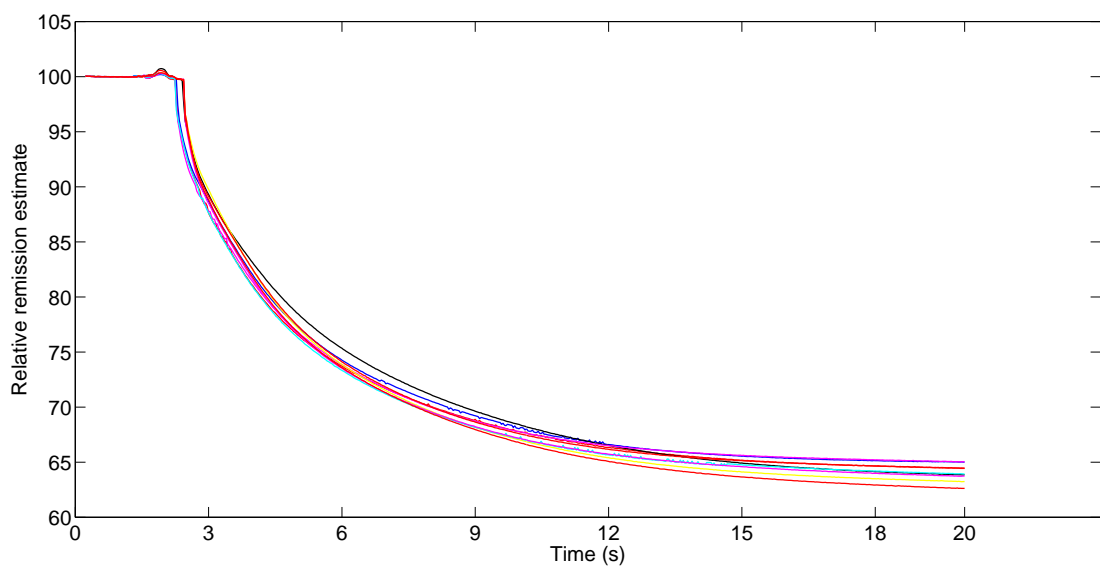


**Figure 7.9:** OTSU Kinetik curve 350 mg/dL.

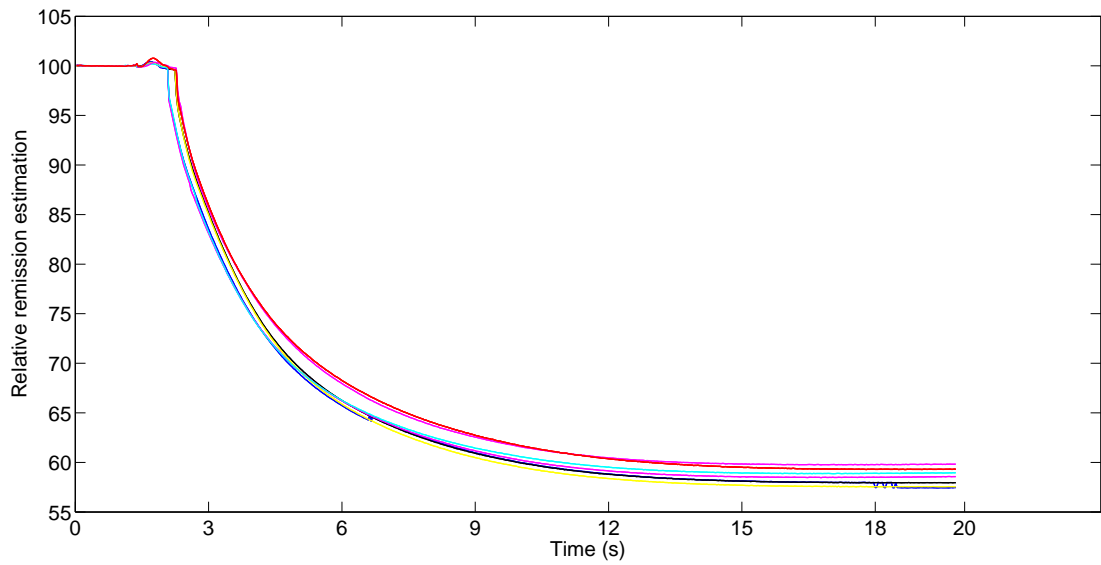


**Figure 7.10:** OTSU Kinetik curve 550 mg/dL.

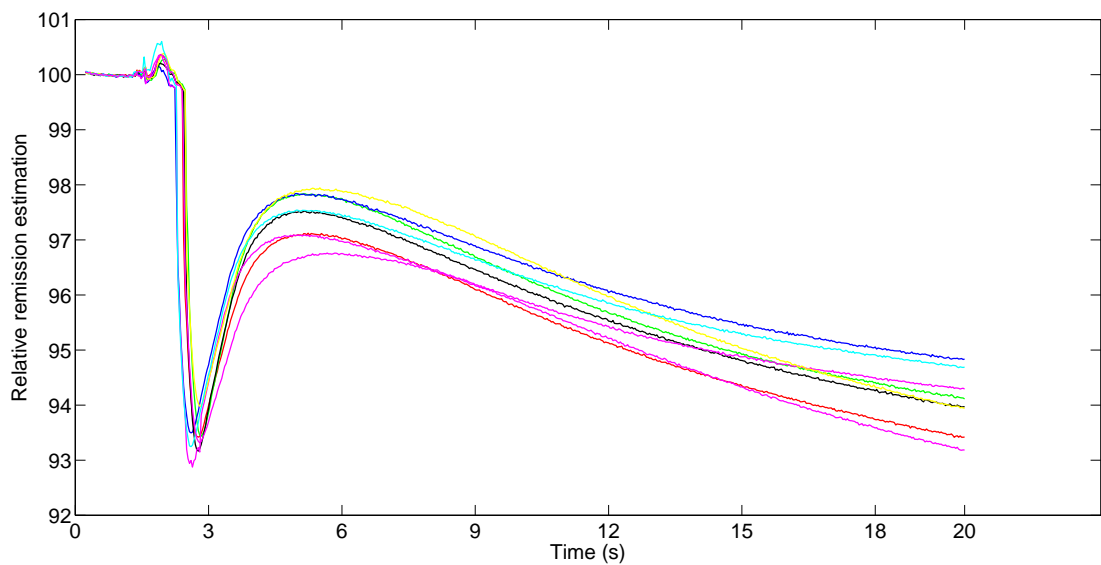


**Figure 7.11:** KDE Kinetik curve 30 mg/dL.

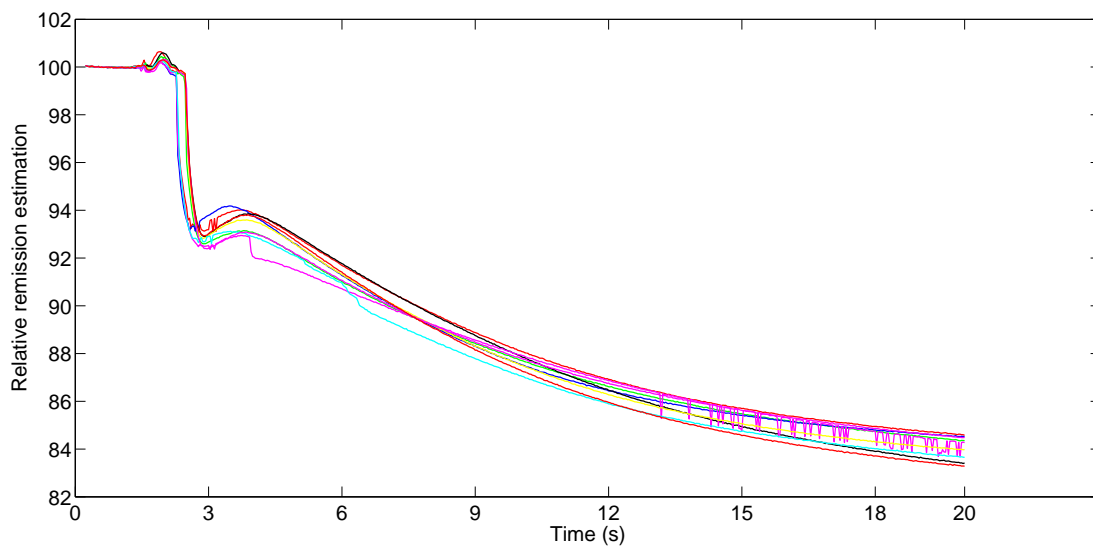


Figure 7.12: KDE Kinetik curve 90 mg/dL.

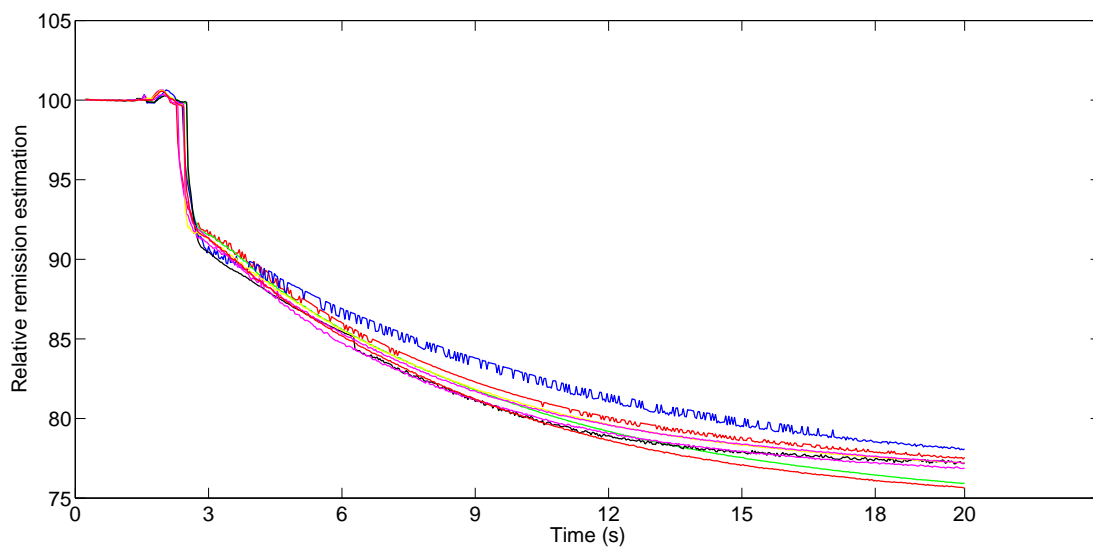
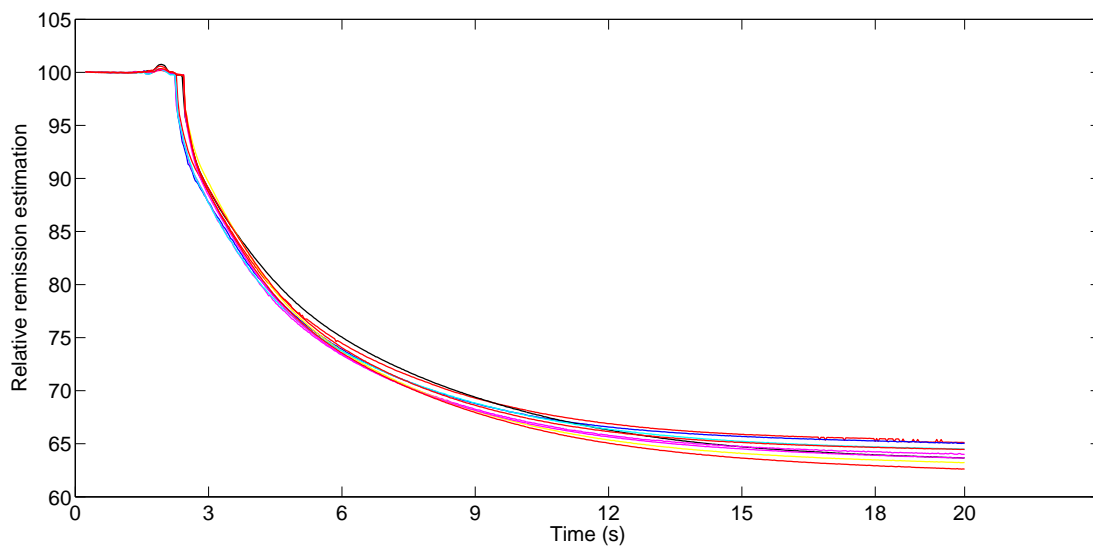
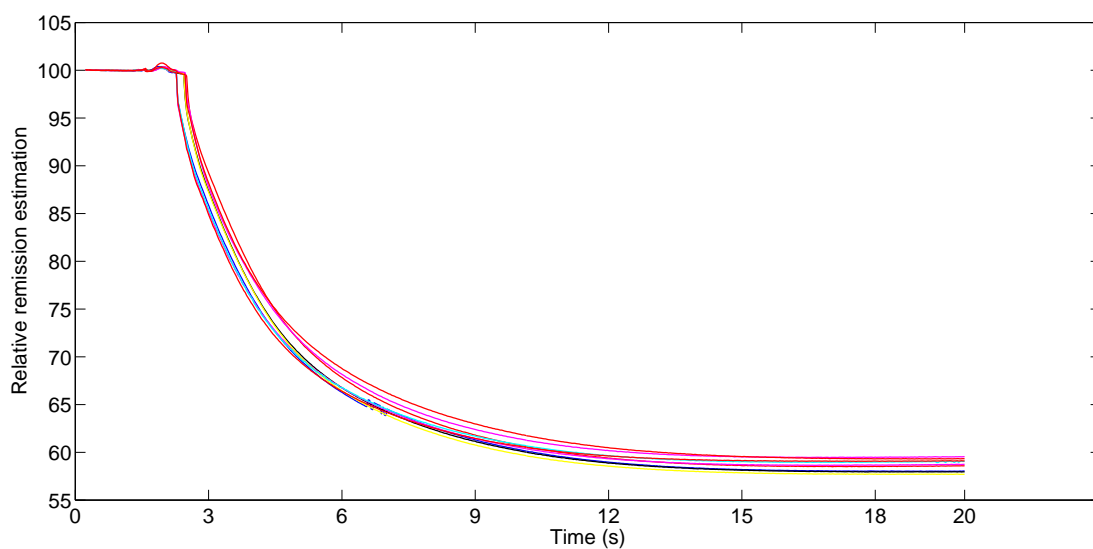


Figure 7.13: KDE Kinetik curve 150 mg/dL.



**Figure 7.14:** KDE Kinetik curve 350 mg/dL.



**Figure 7.15:** KDE Kinetik curve 550 mg/dL.

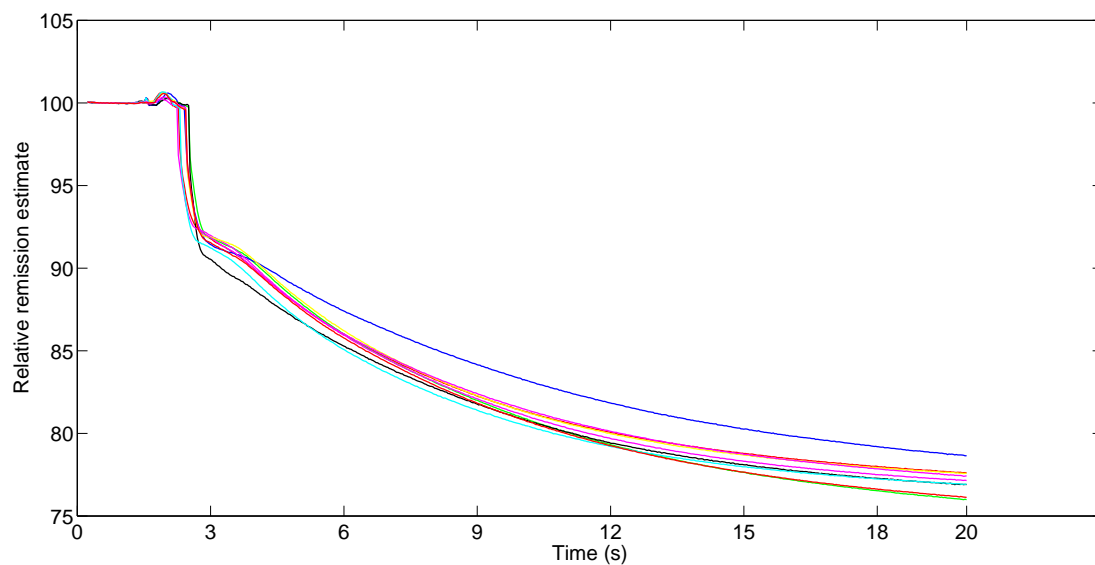


**Figure 7.16:** Watershed segmentation Kinetik curve 150 mg/dL.

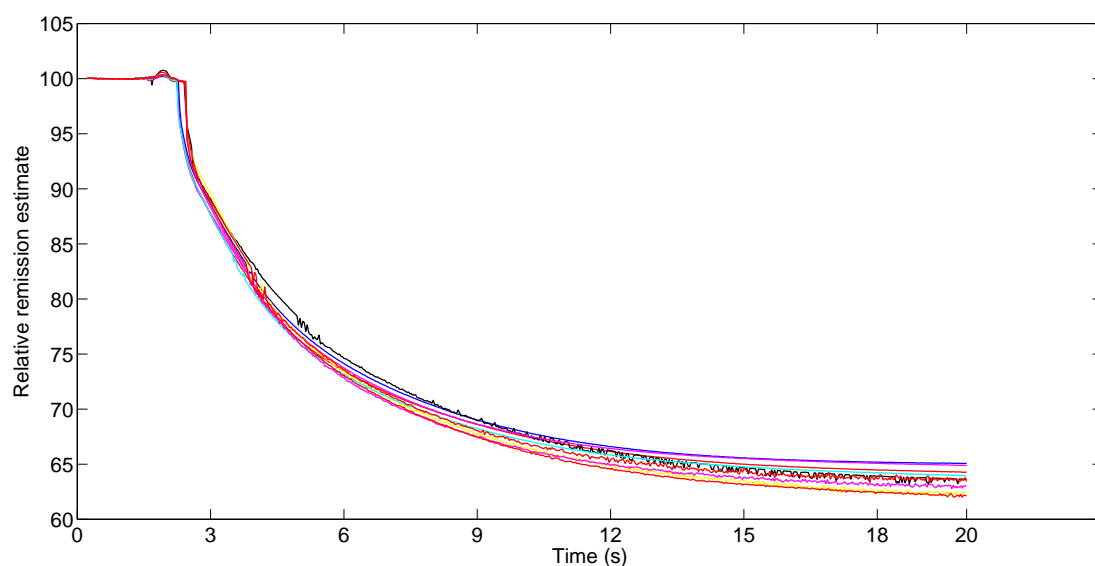


**Figure 7.17:** Watershed segmentation Kinetik curve 300 mg/dL.

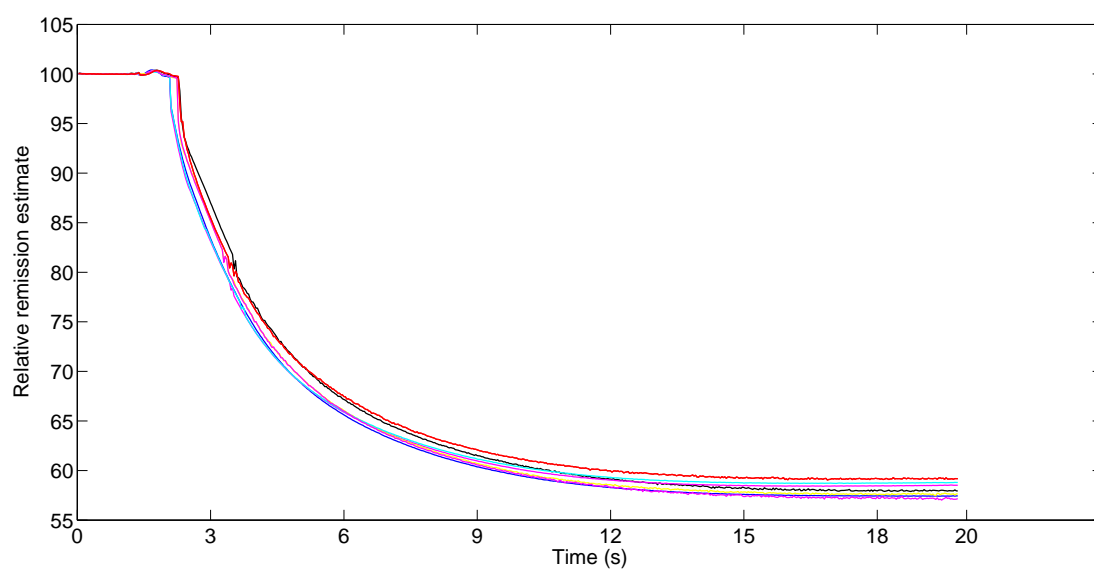


**Figure 7.18:** Watershed segmentation Kinetik curve 550 mg/dL.



---

# Bibliography

- [1] <http://www.idf.org/diabetesatlas/5e/the-global-burden>, retrieved 27. Feb 2013.
- [2] <https://www.accu-chek.co.uk/gb/basics/leaflets.html#top>, retrieved 27. Feb 2013.
- [3] [http://www.emedicinehealth.com/diabetes\\_blood\\_sugar\\_levels-health/article\\_em.htm](http://www.emedicinehealth.com/diabetes_blood_sugar_levels-health/article_em.htm), retrieved 27. Feb 2013.
- [4] Karl Werner Edgar Baumann, Wolfgang Obermeier. *Patent, Light Source Pulsed With Irregular Pulse Sequence in Analog Photometric Signal Evaluation For a Test Carrier Analysis System*. Number 5463467. 1994.
- [5] Rafael C. Gonzalez and Richard E. Woods. *Digital Image Processing*. Addison-Wesley Longman Publishing Co., Inc., Boston, MA, USA, 2nd edition, 2001.
- [6] Rafael C. Gonzalez, Richard E. Woods, and Steven L. Eddins. *Digital Image Processing Using MATLAB, 2nd ed.* Gatesmark Publishing, 2nd edition.
- [7] Nobuyuki Otsu. A Threshold Selection Method from Gray-level Histograms. *IEEE Transactions on Systems, Man and Cybernetics*, 9(1), 1979.
- [8] J. Kittler and J. Illingworth. Minimum error thresholding. *Pattern Recogn.*, 19(1):41–47, January 1986.
- [9] J. M. S. Prewitt and M. L. Mendelsohn. The analysis of cell images. *Ann. N Y Acad. Sci.*, 128(3):1035–1053, 1966.
- [10] W. Härdle, M. Müller, S. Sperlich, and A. Werwatz. *Nonparametric and Semiparametric Models*. Springer Verlag, Heidelberg, 2004.

# A Segmentation Algorithm for Measuring Blood Glucose in Hand-held Devices



TECHNISCHE  
UNIVERSITÄT  
DARMSTADT

*Bachelor-Thesis*

*Veronica Aramendia*

*supervised by Nevine Demitri*



Signal Processing Group

Signal Processing Group

Technische Universität Darmstadt

**upna**  
Universidad  
Pública de Navarra

Nafarroako  
Unibertsitate Publikoa

Todos los derechos reservados  
Eskubide guztiak erresalbatu dira

## Diabetes:

- ▶ Metabolic disease resulting in high blood sugar level.
- ▶ It is expected to affect about 552 million people by 2030.
- ▶ Frequent measuring of blood glucose level is vitally important.

## Challenge:

- ▶ Find the blood sample region. ROI (Region Of Interest).



Introduction.

Methodology.

Proposed Algorithm.

Data Sets and Experimental Results.

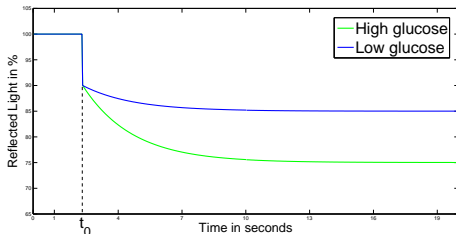
Evaluation and Summary.



# Introduction (cont.)

## Photometric Principle

- ▶ The color reaction is monitored by a camera.
- ▶ Temporal behaviour of the chemical reaction.



$\widehat{rR}$ : Relative remission.

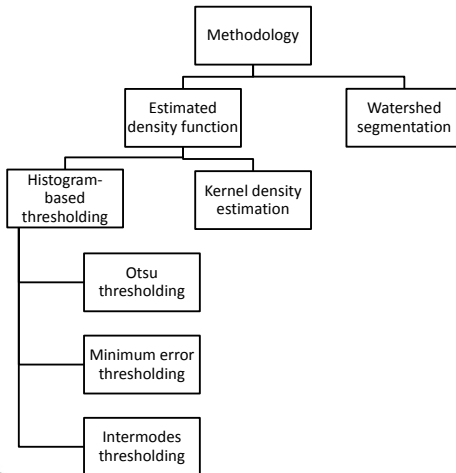
$f_{\text{crnt}}$ : Current frame.

$f_{\text{norm}}$ : Normalized frame.

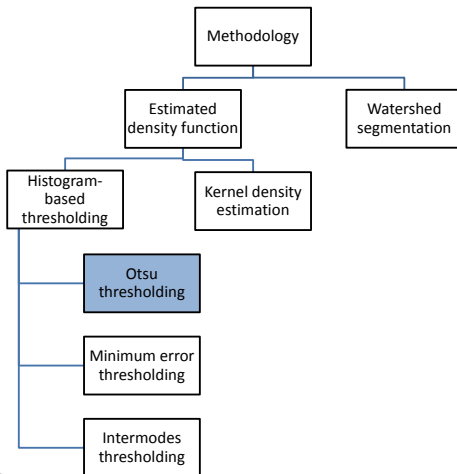
$$\widehat{rR} = \text{reflected light} \left( \frac{f_{\text{crnt}}}{f_{\text{norm}}} \right)$$

- ▶ Find  $t_0$ : Blood sample is detected by the device.

- ▶ Find  $t_{\text{conv}}$



# Methodology: Histograms-based thresholding





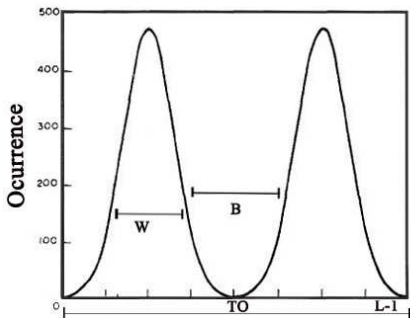
Consider two classes:  $C_0 = (0, \dots, T)$  and  $C_1 = (T + 1, \dots, L - 1)$

## Otsu thresholding

- ▶ **Objective:** Maximize the separability between them.

$$\eta = \frac{\sigma_B^2}{\sigma_{TO}^2};$$

$$\sigma_B^2(T_{\text{opt}}, \text{OT}) = \max_{0 \leq T \leq L-1} \sigma_B^2(T)$$



T: Threshold.

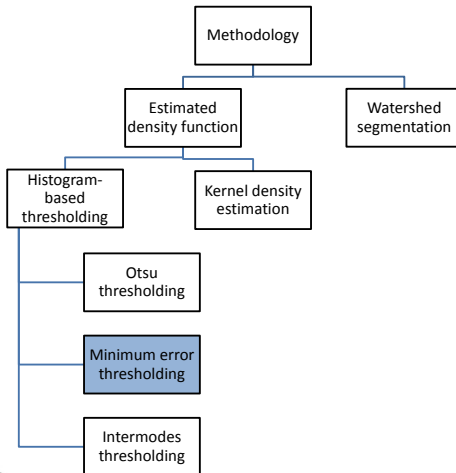
L: Largest grey value.

$\sigma_B^2$ : Between-class variance.

$\sigma_{TO}^2$ : Total variance.

uplia  
Publica de Navarra  
Nafarroako Publikoa  
Todos los derechos reservados  
Eskubide guztiak erresalbatu dira

# Methodology: Histograms-based thresholding



Consider two classes:  $C_0 = (0, \dots, T)$  and  $C_1 = (T + 1, \dots, L - 1)$

## Minimum error thresholding

- ▶ Considers a Gaussian assumption.
- ▶ At a threshold level  $T$ :  $h(I|i, T)$  with parameters  $\mu_i(T)$ ,  $\sigma_i^2(T)$ , and  $P_i(T)$ .

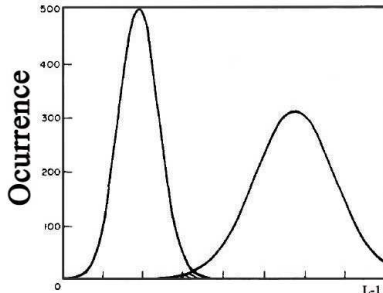
$$J(T_{\text{opt, MET}}) = \min_T J(T);$$

J: Criterion function

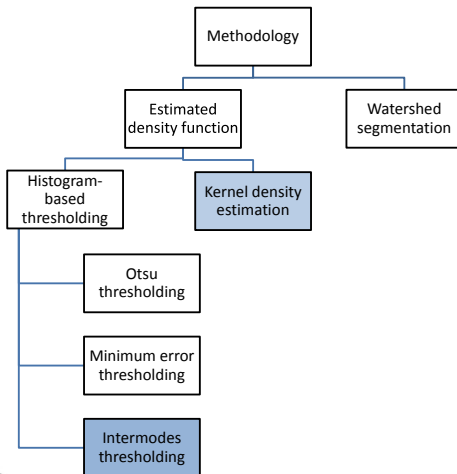
T: Threshold

**upna**  
Universidad  
Pública de Navarra  
Nafarroako  
Unibertsitate Publikoa

Todos los derechos reservados  
Eskubide guztiak erresalbatu dira



# Methodology: Histograms-based thresholding





Consider two classes:  $C_0 = (0, \dots, T)$  and  $C_1 = (T + 1, \dots, L - 1)$

## Intermodes thresholding

- ▶ The histogram is iteratively smoothed until two peaks remain.

$$T_{\text{opt, IM}} = \frac{x_1 + x_2}{2} \quad x_1, x_2 : \text{Local positions of the maximums.}$$

- ▶ Objective: Improve the smoothed intermodes histogram.

## Extension to Kernel density estimation

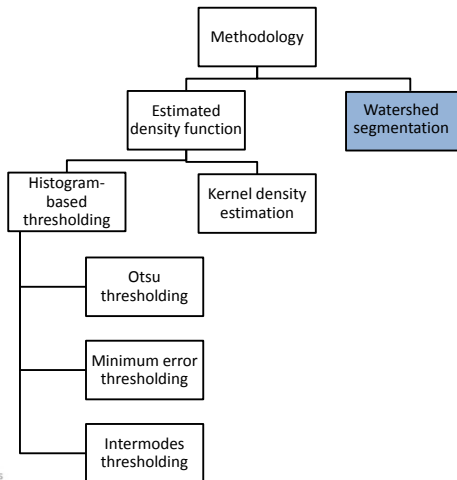
- ▶ It belongs to a non-parametric density estimators.
- ▶ It smooths out the contribution of each data point over a local neighborhood of that data point.

$$\hat{f}_w(\mathbf{x}) = \frac{1}{L \cdot w} \sum_{l=1}^L K\left(\frac{\mathbf{x} - \mathbf{x}_l}{w}\right)$$

$\mathbf{x}$ : Data vector,  $(1, \dots, L)$ .  
 $\hat{f}$ : Estimate density function.  
 $K$ : Kernel function.  
 $w$ : Bandwidth.  
 $\mathbf{x}_1, \mathbf{x}_2$ : Local positions of the maximums.

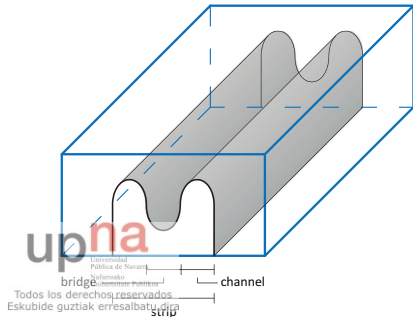
$$T_{\text{opt, KDE}} = \frac{\mathbf{x}_1 + \mathbf{x}_2}{2}$$

# Methodology: Watershed segmentation



## Watershed segmentation

- ▶ Visualizing an image  $I(x, y)$  in three dimensions. Two spatial coordinates  $(x, y)$  and the altitude that corresponds to the gray level of a pixel.

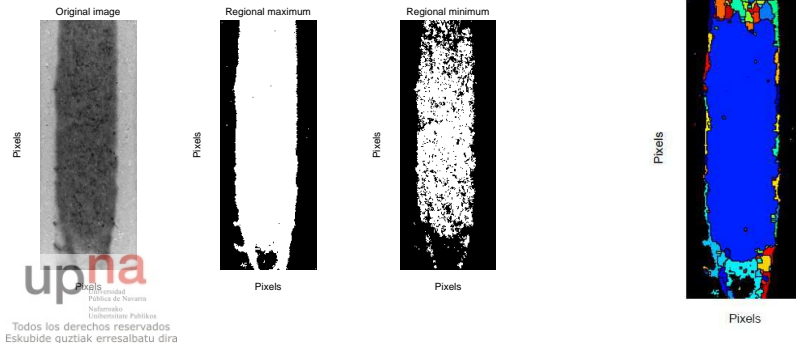


- ▶ **Marker:**  
Connected component belonging to an image.
- ▶ **Distance transform:**  
Distance from every pixel to the nearest non-0 value.

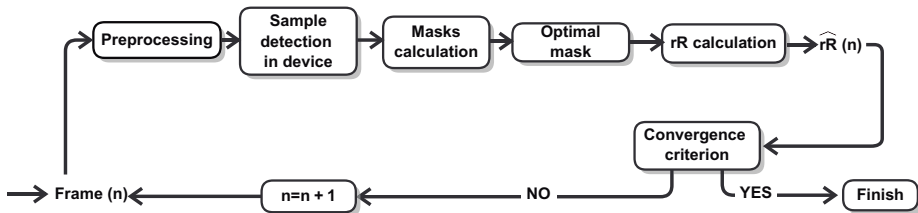


# Methodology: Watershed segmentation (cont.)

- ▶ Preprocessing steps:
  - ▶ Markers.
  - ▶ Distance transform and gradient.
  - ▶ Impose minimums

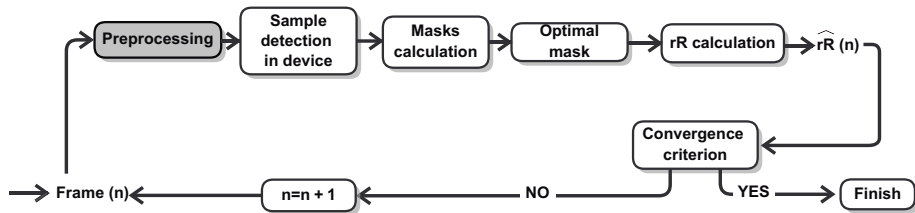


# Proposed Algorithm



# Proposed Algorithm

## Preprocessing.



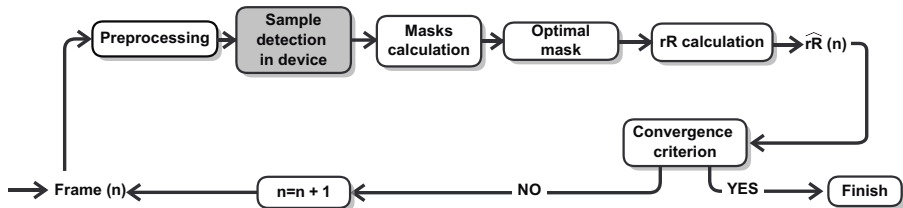
- ▶ Crop.
- ▶ Normalize.

# Proposed Algorithm

## Sample detection in device.



TECHNISCHE  
UNIVERSITÄT  
DARMSTADT



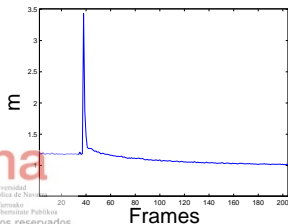
# Proposed Algorithm

## Sample detection in device.

- ▶ Find the start of the reaction:  $t_0$ .

$$m(k) = \frac{1}{M \cdot N} \sum_{i=1}^N \sum_{j=1}^M |I_k(i, j) - I_{k+1}(i, j)|$$

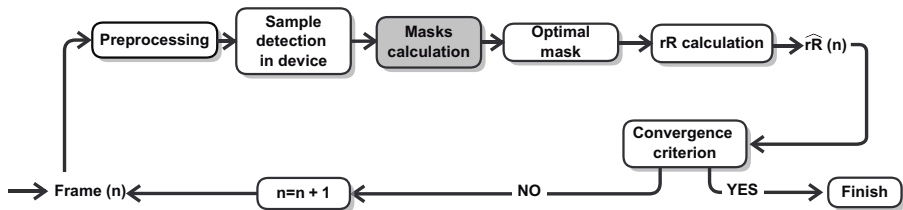
$$\text{SID} = \max(m)$$



k: Number of frames.  
I: Image.  
N,M: Image dimensions.

# Proposed Algorithm

## Masks calculation.



# Proposed Algorithm

## Masks calculation.



- ▶ SID mask.
  - ▶ Represents  $t_0$ .
  - ▶ A contrast logarithmic function is applied to it.
- ▶ TIME mask.
  - ▶ Changes over the time.
  - ▶ Represents the whole frames of the test measurement.

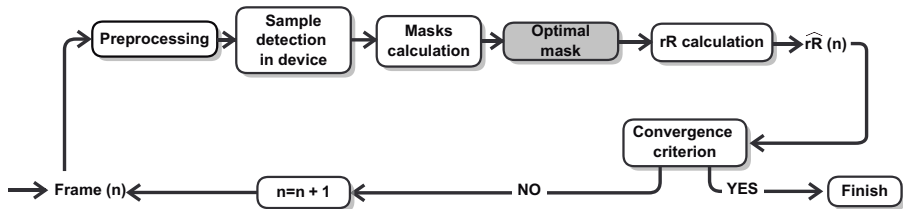
The different thresholding methods and the watershed segmentation are used.



Todos los derechos reservados  
Eskubide guztiak erresalbatu dira

# Proposed Algorithm

## Optimal mask.





# Proposed Algorithm

## Optimal mask.

- ▶ **Criteria:**
  - ▶ Borders of the image.
  - ▶ Total amount of black pixels.
- ▶ The optimal mask is the one with thicker borders.

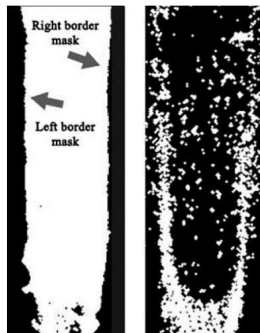
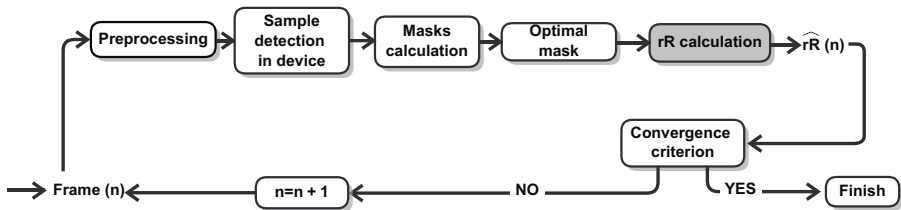


Figure : TIME mask: 550 mg/dL and 30 mg/dL.

# Proposed Algorithm

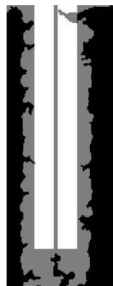
## Relative remission calculation



# Proposed Algorithm

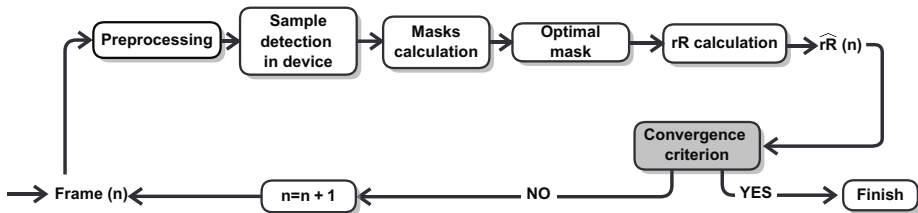
## Relative remission calculation

- ▶ If the optimal mask is the SID mask, minimize.
- ▶ Calculate the mean of the white pixels of the mask.
- ▶ The ROI area must have a minimum number of pixels.



# Proposed Algorithm

## Convergence criterion



- ▶ Convergence takes place when the inter-frame difference is equal or smaller than 1% for three consecutive times in a row.

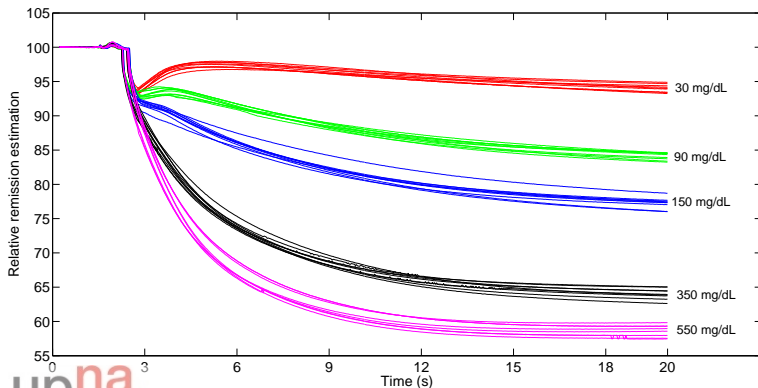


# Experimental Results

## Otsu thresholding method



TECHNISCHE  
UNIVERSITÄT  
DARMSTADT



**upna**  
Universidad  
Pública de Navarra  
Nafarroako  
Unibertsitate Publikoa

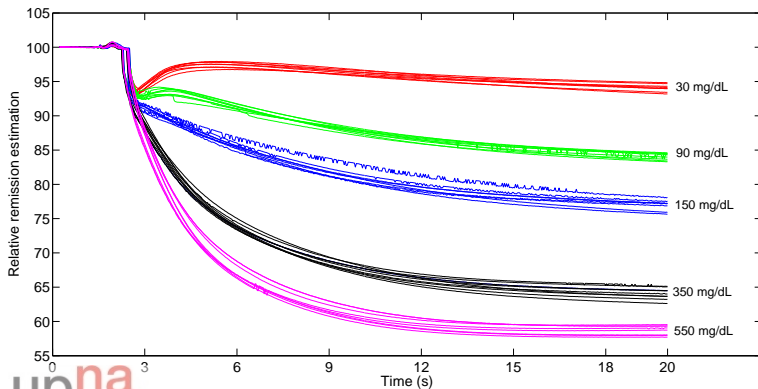
Todos los derechos reservados  
Eskubide guztiak erresalbatu dira

# Experimental Results

## KDE thresholding method



TECHNISCHE  
UNIVERSITÄT  
DARMSTADT

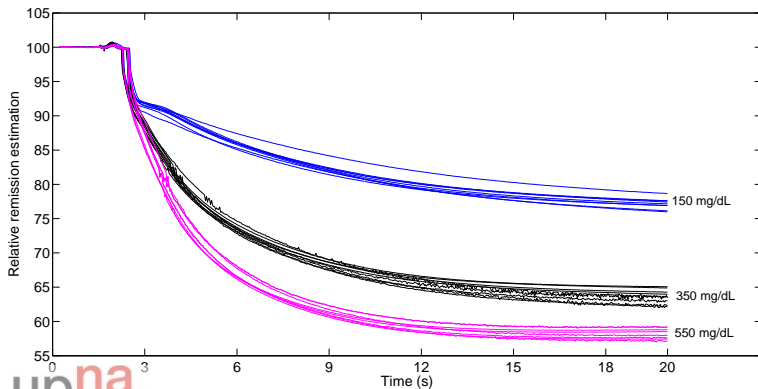


**upna**  
Universidad  
Pública de Navarra  
Nafarroako  
Unibertsitate Publikoa

Todos los derechos reservados  
Eskubide guztiak erresalbatu dira

# Experimental Results

## Watershed segmentation method





# Experimental Results

Variance  $\sigma_{rR}^2$  :

Glucose value	30	90	150	350	550
OT	<b>0.13</b>	1.99	1.04	<b>0.65</b>	0.56
KDE	<b>0.13</b>	<b>0.38</b>	2.55	0.93	<b>0.41</b>
WS	-	-	<b>0.75</b>	2.7	1.4

- ▶ Resolution limit= 0.1

Computation time (s/frame):

Glucose value	30	90	150	350	550
OT	<b>0.24</b>	<b>0.29</b>	<b>0.28</b>	<b>0.27</b>	<b>0.32</b>
KDE	0.29	0.30	0.46	0.33	0.41
WS	-	-	0.31	0.53	0.79

# Evaluation

## Thresholding methods



### Otsu Thresholding (OT)

- ▶ Does not take into account any probability distribution.
- ▶ Gives the correct optimal mask for every frame.

### Minimum Error Thresholding (MET)

- ▶ Problems with images that are not Gaussian distributed.
- ▶ Do not select a good T.

### Intermodes Thresholding (IM)

- ▶ The bimodal histogram of the image typically reflects two unequal peaks.
- ▶ It takes as second maximum a peak presented in the noise tail.

### Extension to kernel density estimation (KDE)

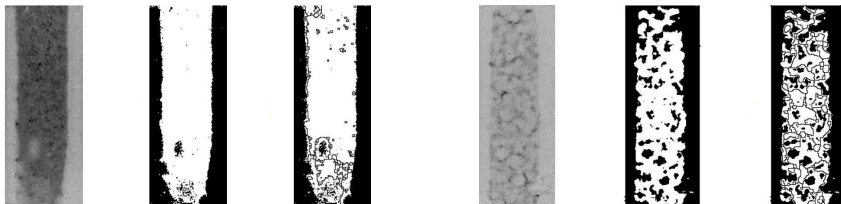
- ▶ Calculates an accurate smoothing histogram, despite the unequal peaks.

# Evaluation

## Watershed segmentation

### Watershed segmentation

- ▶ Problems in low glucose values.
- ▶ If we compare the masks of Otsu and Watershed for higher and lower glucose, we get:





## Summary

- ▶ Algorithms implementation for the thresholding operators.
- ▶ Comparison of the different methods.
- ▶ OT method and KDE outperform the others in time and accuracy.

## Outlook

- ▶ Try new segmentation methods.
- ▶ Achieve higher accuracy in the optimal mask calculated.
- ▶ Propose new solutions for lower glucose values.



Universidad  
Pública de Navarra  
Nafarroako  
Unibertsitate Publikoa

Todos los derechos reservados  
Eskubide guztiak erresalbatu dira



Thank you for your attention!



TECHNISCHE  
UNIVERSITÄT  
DARMSTADT

upna

Universidad  
Pública de Navarra

Nafarroako  
Unibertsitate Publikoa

Todos los derechos reservados  
Eskubide guztiak erresalbatu dira

### MSE(Mean Squared Error)

- ▶ Combines the Variance and the squared Bias.

$$MSE(\hat{f}_w(x)) = \text{Var}(\hat{f}_w(x)) + \text{Bias}(\hat{f}_w(x))^2$$

- ▶ Find  $w$  that minimizes MSE:
  - ▶ Neither oversmoothed (large bandwidth value) -> Variance
  - ▶ Bias: Nor undersmoothed (small bandwidth) -> Bias

### MISE(Mean Integrated Squared Error)

- ▶ Global measure of estimation accuracy

$$MISE(\hat{f}_w) = \text{mean} \left[ \int_{-\infty}^{+\infty} \{\hat{f}_w(x) - f(x)\}^2 dx \right]$$



## AMISE (Asymptotic Mean Integrated Squared Error).

- ▶ Doesn't depend on the unknown density function.

$$w_{\text{opt}} = \arg_{\min}(\text{AMISE})$$



### AMISE Histogram.

$$AMISE(\hat{f}_w) = \frac{1}{n \cdot w} + \frac{h^2}{12} \|f'\|_2^2$$

### AMISE KDE.

$$AMISE(\hat{f}_w) = \frac{1}{n \cdot w} \|K\|_2^2 + \frac{w^4}{4} \cdot \{\mu_2(K)\}^2 \|f''\|_2^2$$

### Dependence on the origin

- ▶ Compute the histograms using the same binwidth but different origins and to average.
  - ▶ ASH (Average Shifted Histogram)
- ▶ number of bins  $\rightarrow \infty$ , ASH is not dependent on the origin anymore and converts into a continuous function.

## Otsu thresholding

- ▶ Zero and first order cumulative moments:

$$\omega(T) = \sum_{l=0}^T p_l; \quad \mu(T) = \sum_{l=0}^T l \cdot p_l;$$

- ▶ Between class variance:

$$\eta = \frac{\sigma_B^2}{\sigma_{TO}^2}; \quad \sigma_B^2 = \frac{(\mu_{TO}\omega(T) - \mu(T))^2}{\omega(T)[1 - \omega(T)]}$$



## Minimum error thresholding

- ▶ The  $\mu_i$ ,  $\sigma_i^2$  and  $P_i$  can be estimated. At a certain threshold T:

$$P_1(T) = \sum_{l=0}^T h(l); \quad \mu_1(T) = \left[ \sum_{l=0}^T h(l)l \right] / P_1(T);$$

$$\sigma_1^2(T) = \left[ \sum_{l=0}^T \{l - \mu_1(T)\}^2 h(l) \right] / P_1(T);$$

$$J(T) = \sum_{l=0}^{L-1} h(l) \cdot \epsilon(l, T)$$

$\mu_i$ : Mean

$\sigma_i$ : Standard deviation

$P_i$ : Prior probability

$h$ : Histogram

$l$ : Gray level  $l$ th.

Uptia  
Publica de Navarra

Navarra  
Universidad Pública

Todos los derechos reservados

Estudiorik guztiak erresaltatu dira